

Hepatic Vein Segmentation in CT Images using Fast  
Marching Method Driven by Gaussian Mixture Models

SONG ZHIYUAN

(B.Sc., ZHEJIANG UNIVERSITY, 2003)

A THESIS SUBMITTED  
FOR THE DEGREE OF MASTER OF SCIENCE  
DEPARTMENT OF COMPUTER SCIENCE  
SCHOOL OF COMPUTING

NATIONAL UNIVERSITY OF SINGAPORE

2010

## Acknowledgements

First of all, I would like to express my sincere gratitude to my supervisor, Assoc. Prof. Leow Wee Kheng, for his instructive advice and useful suggestions on my thesis. I am deeply grateful of his help in the completion of this thesis. I am also deeply indebted to all colleagues in Computer Vision Laboratory, National University of Singapore. I really enjoyed the pleasant stay with these brilliant people for the past 4 years. Special thanks should go to my friends who have put considerable time and effort into their comments on the draft. Finally, I am indebted to my parents for their continuous support and encouragement.

# Contents

<b>1</b>	<b>Introduction</b>	<b>1</b>
1.1	Motivation . . . . .	1
1.2	Thesis Objective . . . . .	3
1.3	Thesis Organization . . . . .	4
<b>2</b>	<b>Background</b>	<b>5</b>
2.1	Liver Anatomy . . . . .	5
2.2	Liver CT Images . . . . .	8
<b>3</b>	<b>Related Work</b>	<b>11</b>
3.1	Centerline-based Approaches . . . . .	11
3.2	Region-based Approaches . . . . .	14
3.2.1	Region Growing Approaches . . . . .	14
3.2.2	Morphological Operator-based Algorithm . . . . .	17
3.3	Boundary-based Approaches . . . . .	20
3.3.1	Snake . . . . .	20
3.3.2	Level Set . . . . .	23
3.3.3	Parametric Model-based Approaches . . . . .	28

<i>CONTENTS</i>	4
3.4 Summary . . . . .	33
<b>4 Fast Marching Method Driven by Gaussian Mixture Models</b>	<b>35</b>
4.1 Problem Description . . . . .	36
4.1.1 Input Data . . . . .	36
4.1.2 Overview of Algorithms . . . . .	36
4.2 Hepatic Vein Segmentation Algorithm . . . . .	38
4.2.1 Noise Removal . . . . .	38
4.2.2 Hepatic Vein Segmentation Using Fast Matching Method	40
4.2.3 Vena Cava Removal . . . . .	46
4.3 Performance Measure . . . . .	50
<b>5 Conclusion and Future Work</b>	<b>57</b>

## **Abstract**

Liver cancer is a serious disease in human beings. An effective way to cure liver cancer is the liver transplant operation. However, to make the surgical plan, the doctors need to know the structure, location and thickness of the hepatic vein. Therefore, hepatic vein segmentation is an initial and crucial step in liver cancer surgery.

This thesis focuses on segmentation of hepatic veins from abdominal CT images. The purpose of this work is to obtain a volumetric hepatic vein model from the abdominal CT for liver transplant operation. To solve this problem, this thesis proposes a fast marching method driven by Gaussian mixture models (GMM) to segment hepatic vein from CT images. Anisotropic smoothing is applied to the original CT data to remove the noise. After that, GMMs are built for both hepatic vein area and non-hepatic vein areas based on hand-draw sampling points. The fast-marching propagation speed at each location is controlled by the generated GMMs. After that, a parametric cylinder model based algorithm is proposed to remove the unnecessary vena cava from the segmentation result. The segmentation results are analyzed and discussed.

# Chapter 1

## Introduction

### 1.1 Motivation

Liver cancer is a serious disease in human beings, and it is the third commonest cancer followed by stomach cancer and lung cancer. As reported in the Annual Statistics Reported on Causes of Death in 2004, an average of 23.1 out of 100,000 USA people died of liver cancer [27]. If the patient's whole liver is spoiled and cannot function anymore, The patient requires to plant new liver tissue from other people through transplantation.

Liver transplant operation is such an operation that removes the whole damaged liver from the patient and transplants a new and health liver tissue into the patient's body.

When transplanting part of liver from the donator to the patient, the cutting path on the liver must be carefully designed based on the anatomy of the patient's liver organ in order to minimize damage to the liver vasculature. The less the liver vasculature is damaged, the faster the transplanted

liver tissue grows. So before the operation, surgeons must obtain accurate information of the liver blood vessels, especially hepatic vein and portal vein, which can help them to decide the liver cutting path. This information can be obtained from liver CT images. Therefore, the segmentation of liver blood vessels in CT images plays a crucial role in liver transplant operation.

Many segmentation algorithms have been designed for blood vessel segmentation in the last few decades. They can be categorized into three groups: centerline-based approaches, region-based approaches and boundary-based approaches. However, none of these algorithms can segment tree-structured blood vessels well from CT images. Centerline-based approaches extract blood vessel centerlines and then connect the centerlines to form the vessel tree, but they usually require a large amount of user inputs. The users is required to mark the start and end points for each vessel branch, which makes it impossible to segment complex vessel trees. Region-based approaches try to accumulate all image voxels that belong to the blood vessels, but they are sensitive to noise and suffer from serious leakage problems. Boundary-based approaches employ some parametric models to fit the boundaries of the blood vessels in CT images, but they always require high computational cost, and the output result is highly dependent on good initialization. As a result, semi-automatic segmentation is still widely used in real medical applications, which is rather tedious and time consuming. Therefore, new segmentation algorithm is required to segment liver blood vessels in CT images.

## 1.2 Thesis Objective

The objective of this thesis is to develop an algorithm for segmenting and reconstructing 3D volumetric model of the hepatic veins from CT images.

The algorithm requires all the features below:

- The algorithm should produce a correct segmentation result of hepatic veins, including left hepatic vein, right hepatic vein and middle hepatic vein.
- The algorithm can produce a 3D volumetric model of the hepatic vein. The relative location, orientation, thickness and connecting information of each bifurcate vessel branches should be accurate enough for the purpose of surgery planning.
- The algorithm should be effective and efficient.
- The algorithm should also require few user inputs and easy to use.

The main contribution of my thesis is that I develop an algorithm to segment the tree-structured hepatic veins from CT images. It can segment main branches as well as bifurcate branches of the hepatic vein at the same time and it does not require specific initialization for each vessel branch. My algorithm only requires a small amount of user inputs. Thus the doctors can process each patient's data and determine the surgical plan in a short period of time. My algorithm can remove vena-cava from the segmentation result, which may be wrongly segmented by other algorithms such as level-set and region growing.

## 1.3 Thesis Organization

To understand the difficulties and detailed requirements of hepatic vein segmentation problem, it is necessary to discuss the liver anatomy first (Chapter 2). Then existing blood vessel segmentation algorithms are reviewed in Chapter 3, including centerline-based approaches (Chapter 3.1), region-based approaches (Chapter 3.2) and boundary-based approaches (Chapter 3.3). Pros and cons of these approaches are analyzed in Chapter 3.4. My algorithm will be introduced in Chapter 4. Experiment results and comparison are also given in Chapter 4. Chapter 5 concludes the whole thesis finally.

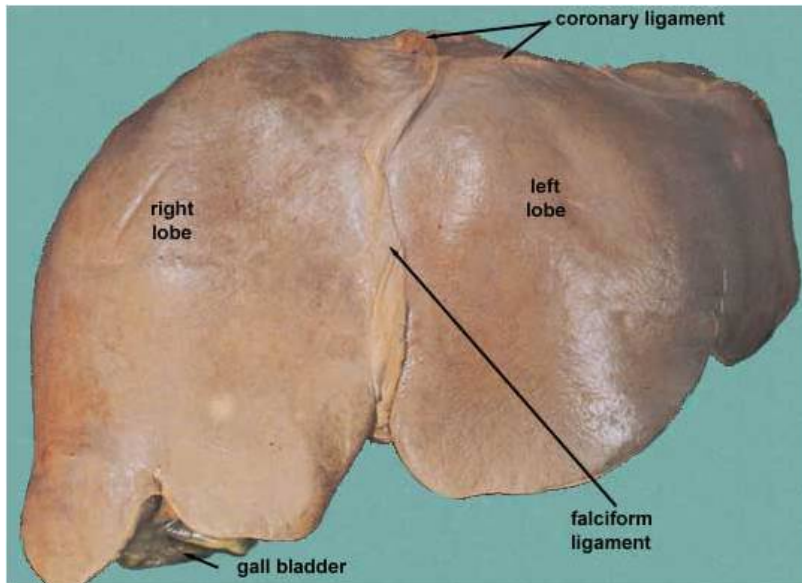
# Chapter 2

## Background

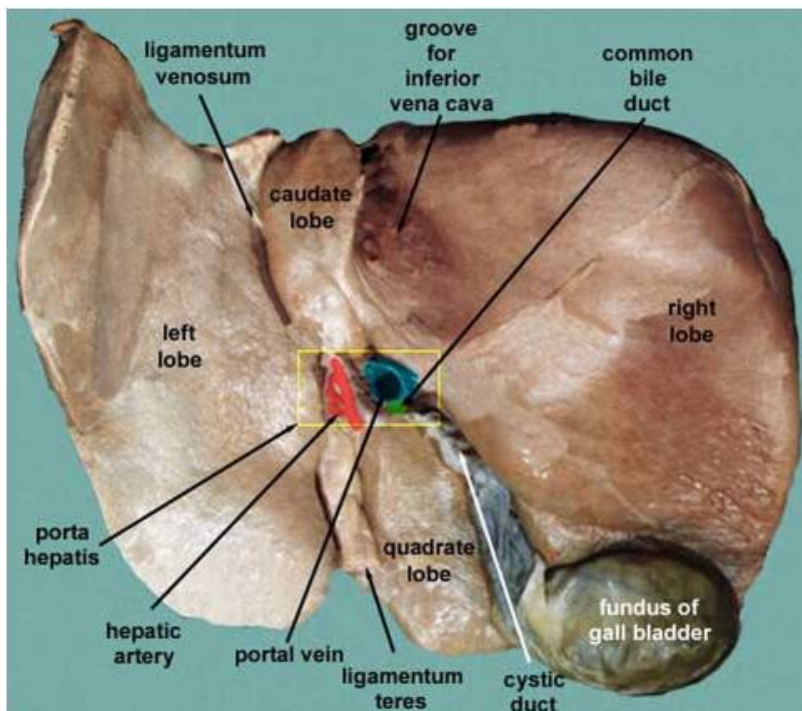
### 2.1 Liver Anatomy

The classical descriptive anatomy nomenclature divides the liver into 4 lobes, namely right, left, caudate and quadrate, based on external ligament visible on the surface of the liver [38]. Right and left lobes are separated by the falciform ligament on the anterior surface of the liver. On the inferior and posterior surfaces, an H-shaped group of fissures and fossae delimits the four lobes. Figure 2.1 shows the anterior and inferior views of a human liver, in which the four lobes are marked.

Another nomenclature widely accepted by hepatic surgeons currently is based on internal vascular and biliary architecture of the organ [38]. Internal vascular includes hepatic veins, portal veins, gallbladder and so on. In this nomenclature, the liver is divided into eight segments, each of which has a branch of the portal vein at its center and a hepatic vein at its periphery. Figure 2.2 illustrates the front view of the eight segments. As can be seen,



(a)



(b)

Figure 2.1: The four lobes of the liver. Images are downloaded from <http://home.comcast.net/WNOR/liver.htm>. (a) Anterior view of the liver. (b) Inferior view of the liver.

Segment Two to Segment Four belong to the left lobe, and Segments Five to Segment Eight belong to the right lobe. Segment One is the caudate lobe which cannot be seen from the front.

Hepatic vein is the blood vessel that drain de-oxygenated blood from the liver back into heart through inferior vena cava (IVA). In liver anatomy, hepatic vein has three main branches, whose roots are connected with inferior vena cava. The three main branches propagate some tiny branches, which go deeply into the eight segments of the liver. As can be seen in Figure 2.2, the thick and straight tube is the inferior vena cava, and the three blue branches are the hepatic vein, namely left, middle and right hepatic vein.

The portal vein is a blood vessel in the liver that drains blood from the digestive system and its associated glands. In liver anatomy, the main portal vein has two main branches, called left portal vein and right portal vein. The left portal vein initially come into the caudate lobe, which is Segment one of the liver. Then it divided into two branches. The ascending branch of the left portal vein then travels anteriorly in the left intersegmental fissure to divide the medial and lateral segments of the left lobe. The right portal vein has an anterior branch that lies centrally within the anterior segment of the right lobe and a posterior branch that lies centrally within the posterior segment of the right lobe [38]. As can be seen from the lower part of Figure 2.2, the purple vasculature denotes the portal vein.

Hepatic artery is a short and thin blood vessel that supplies oxygenated blood to the liver. Seen from Figure 2.2, the thin red blood vessel in the lower part of the figure denotes the hepatic artery. It is not important in liver surgery, so it will not be discussed in details in this thesis.

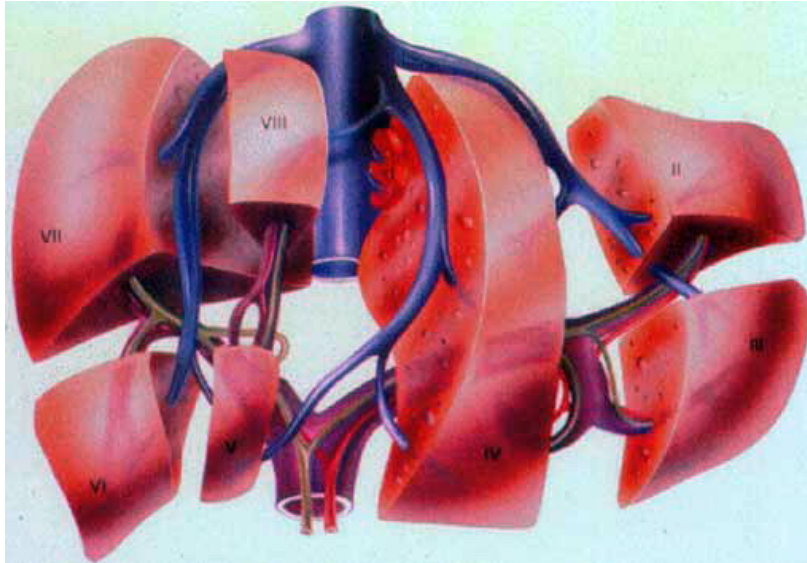


Figure 2.2: Diagram of the liver segments (I-VIII) with their portal venous branches (violet), separated by hepatic veins (blue branches) and the transverse fissure. Segments are numbered in a counterclockwise direction. Segment 1 is the caudate lobe which cannot be seen from the front [38].

## 2.2 Liver CT Images

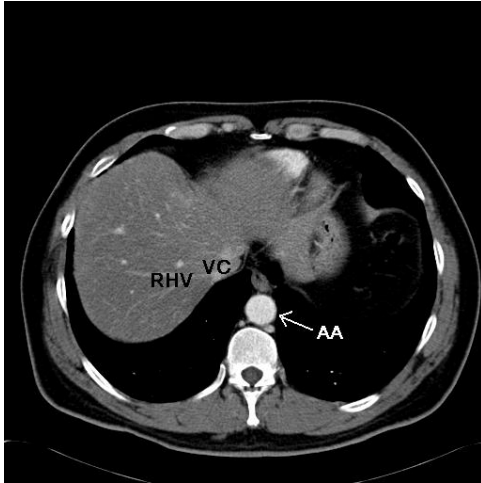
For a better understanding on the segmentation requirement and difficulties on liver blood vessel segmentation, four CT image slices are shown in Figure 2.3 They are acquired from one patient, and shown in top-bottom order.

As can be seen from the images, the white ellipse in the middle of all four image slices is the abdominal aorta, which is a thick and straight blood vessel in abdomen. The gray ellipse lies on top-left of abdominal aorta is the inferior vena cava. Abdominal aorta and inferior vena cava can be seen in all liver CT slices.

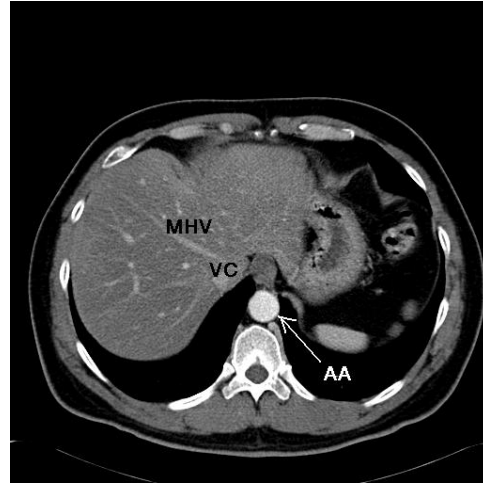
Hepatic veins are vessel branches connecting the inferior vena cava. As can be seen in Figure 2.3(a) and Figure 2.3(b), the two branches are right

and middle hepatic vein, which connect the inferior vena cava. Left hepatic vein cannot be seen here.

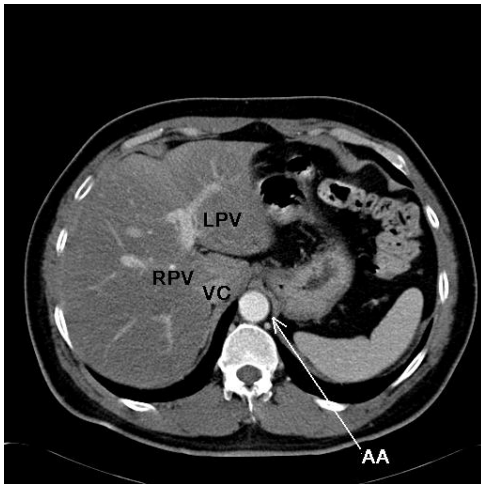
The main branches of the portal veins always occur at the lower part of the liver. Seen from Figure 2.3(c) and Figure 2.3(d), the entrance of the portal vein is a gap between live lobes. And the right and left portal vein always form a 'H' shape.



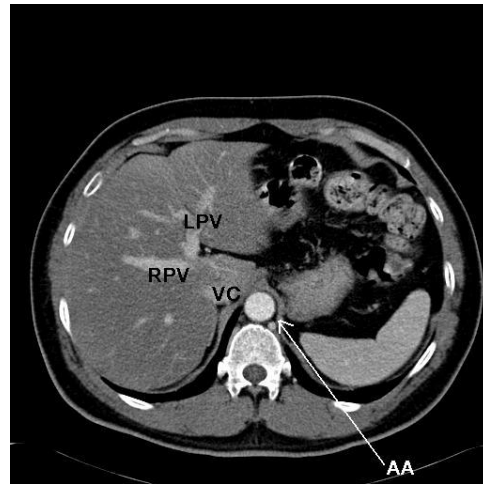
(a)



(b)



(c)



(d)

Figure 2.3: Four CT slices of the liver. Slices are shown in top-bottom order. Abdominal aorta (AA), inferior vena cava (VC), right hepatic vein (RHV), middle hepatic vein (MHV), right portal vein (RPV) and left portal vein (LPV) are marked in the slices. Data collected from National University Hospital, Singapore.

# Chapter 3

## Related Work

Vasculature segmentation on medical images is an essential step in medical diagnosis and surgery. However, segmentation methods vary depending on the imaging modality, application domain, method being automatic or semi-automatic, and other specific factors. Generally, current vasculature segmentation methods can be categorized into three groups as follows:

- Centerline-based approaches
- Region-based approaches
- Boundary-based approaches

### 3.1 Centerline-based Approaches

The main idea of centerline-based approaches is to extract the vasculature centerlines from the images and then reconstruct the vasculature tree by connecting all the centerlines. Figure 3.1 shows an example of coronary

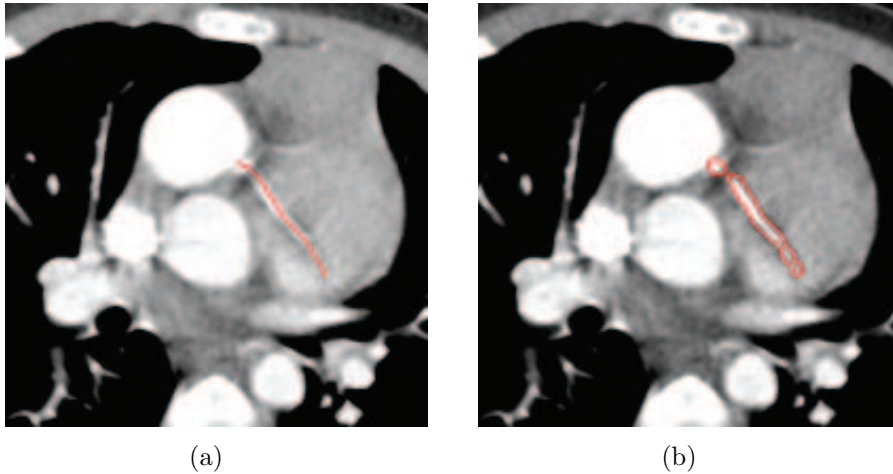


Figure 3.1: An example of coronary artery segmentation using centerline-based method [30]. (a) the extracted centerline. (b) the segmentation result

artery segmentation using centerline-based approaches. The centerline is first extracted from the image data, and then the boundary of the coronary artery is obtained by some fitting procedure.

Different techniques can be applied to extract the centerlines. Niki *et al.* [22] uses thresholding and 3D object connectivity procedure to obtain the blood vessel centerlines. Tozaki *et al.* [39] extract the centerline by applying the thresholding followed by a thinning procedure. The thinning procedure erodes the thresholding result until one voxel thickness. Kawata [16, 17] uses a graph description procedure to extract the curvilinear centerlines of the vasculature. Their procedure consists of three steps: thresholding, elimination of the small connected components and then a 3D fusion process.

Sorantin *et al.* [37] proposed a 3D centerline detection method to segment tracheal stenoses in spiral CT images based on fuzzy connectedness theory. First, the tracheal stenoses is roughly segmented using fuzzy connectedness.

Tracheal stenoses is extracted as a single object started from a user-supplied seed point. Then a 3D dilation procedure is applied to handle the uncertain boundary points due to partial volume effect. Second, a 3D thinning operation is applied to the segmented tracheal stenoses. In the third step, the centerline is obtained using a shortest path searching algorithm. Here the begin and end points of the centerline should be manually marked. Then a smooth procedure is applied to the centerline. Finally the cross-sectional diameter of the vessel is calculated.

Aylward *et al.* [3], Bullitt [2], Chandrinou [5], Florin [9] and Guo [13] use ridge-based methods to extract the centerlines. Ridge-based methods treats the gray-scale images as 3D elevation maps in which intensity ridges approximate the skeleton of the tubular objects (See Figure 3.2). After creating the elevation map, ridge points are local peaks and can be detected. The ridge based centerline detection algorithm consists of four steps. In the first step, the elevation map is created based on image intensity. In the second step, a seed point is manually marked as the starting point. In the third step, an ridge point can be obtained by tracing the elevation map from the seed point along the steepest ascent direction until reaching the local peak. In the fourth step, the entire centerline can be obtained by tracing from the ridge point in step three along the tangent direction.

Centerline based approaches have two advantages. First, it can get the structure information of the vascular structure. So it can be used to segment complex tree structured blood vessels. Second, centerline based approaches do not need specific initialization. However, centerline based approaches are sensitive to noise, which makes them impossible to extract all tiny blood

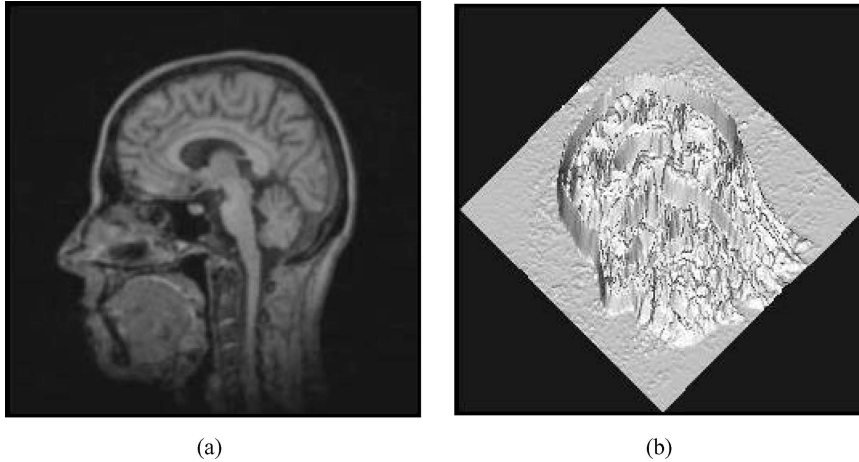


Figure 3.2: An example of the elevation map [3]. (a) An MRI brain image slice. (b) Its corresponding elevation map in 3D.

vessels in medical images such as CT and MRI where noise occurs. Moreover, besides the blood vessel centerline extraction, the blood vessel surface reconstruction procedure is also an important issue in blood vessel segmentation area. Therefore centerline based approaches are always combined with other sophisticated segmentation approaches such as geometric model based approaches.

## 3.2 Region-based Approaches

### 3.2.1 Region Growing Approaches

Region growing approaches segment object of interests by starting from some seed points and incrementally recruiting image pixels to a region based on some predefined criteria. Value similarity and spatial proximity [14] are two important segmentation criteria. It assumes that the neighboring pixels that

have similar intensity belong to the same object.

Region growing approaches are widely applied in vasculature segmentation. Yim *et al.* [45] segments vessel tree structure from MR angiogram using ordered region growing methods, which can resolve the ambiguities in the tree branching due to vessel overlap by incorporating a prior knowledge about the bifurcation spacing. Schmitt *et al.* [31] uses region growing methods combined with thresholding to segment vessels from 3D rotational XRA image volumes.

O'Brien *et al.* [23] uses region growing method to segment coronary arteries from temporal angiogram sequence. Their algorithm consists of three steps. In the first step, a seed point is manually given, and the coronary arteries are approximately segmented using region growing. The thresholding value is given by experience. In the second step, the centerline of coronary arteries are obtained by balloon test. In the third step, the noise are removed by interpolating spatial and temporal connectivity information into the angiogram sequence. Figure 3.3 shows an example of O'Brien's approach. All their segmentation are done in 3D.

Region growing approaches have at least two advantages. They are capable of correctly segmenting regions that have the same properties and are spatially separated, and they generates connected regions. However, region growing approaches have some limitations. First, the segmentation result is highly dependent on the definition of homogeneity criteria. If it is not properly chosen, the regions may leak out into other regions or merge with other regions out of the object of interest. Second, it is difficult to determine the homogeneity criteria in images with low contrast. Therefore, region grow-

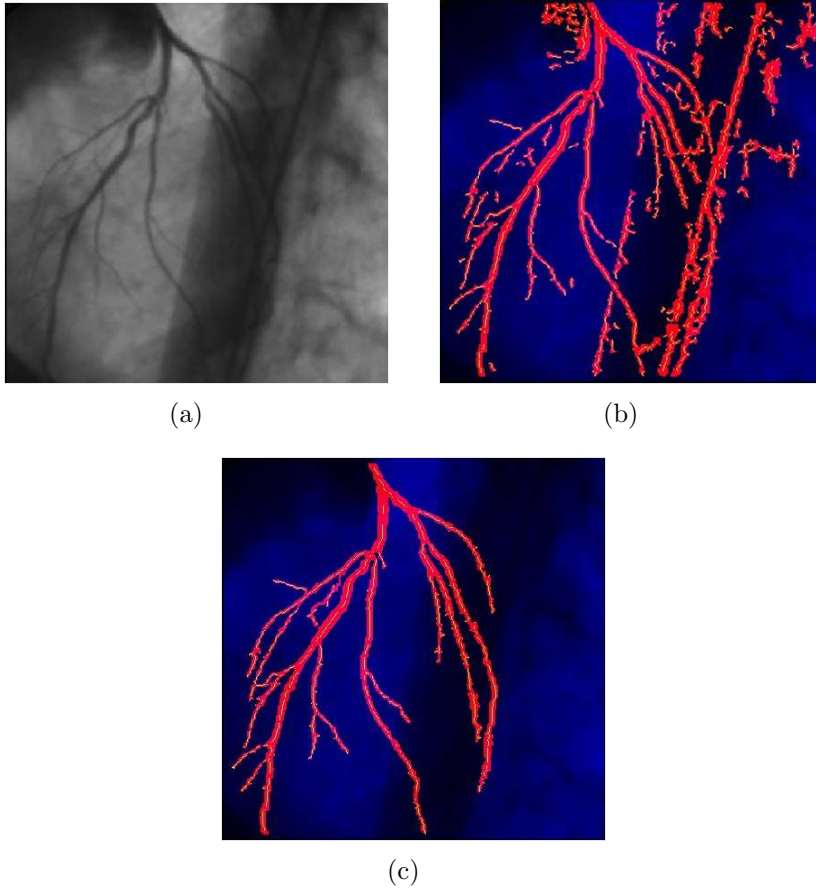


Figure 3.3: An example of coronary artery segmentation using region growing method [23]. (a) The original image. (b) The intermediate segmentation result using region growing. (c) The final result after interpolating spatial and temporal connectivity information.

ing approaches cannot work well on CT and MR images compared with angiogram. Third, region growing approaches are sensitive to the noise, causing extracted regions to have holes or even become disconnected. To overcome this drawback, homotopic region growing approach [10] is proposed, in which the structure information between an initial region and an extracted region is preserved. Fuzzy analogies to region growing have also been developed [11].

### 3.2.2 Morphological Operator-based Algorithm

The main idea of morphological operator based algorithm is to detect the object forms or shapes from the images based on a set of pre-defined structuring elements. Usually a set of structuring elements is defined based on the prior knowledge, then some morphological operators apply structuring elements to images. Dilation and erosion are the two main morphological operators. Dilation expands objects by a structuring element, filling holes, and connecting disjoint regions. Erosion shrinks objects by a structuring element.

A lot of segmentation methods have been proposed using morphological operator. Trackray [40] uses morphological operators to segment vascular structures with a set of eight morphological operators, each of which represents an oriented vessel segment. Figueiredo [8] uses morphological edge detector to segment vessel contours in XRA angiogram. Eiho [6] proposed a method using *top-hat* operator to segment coronary arteries from cine-angiogram.

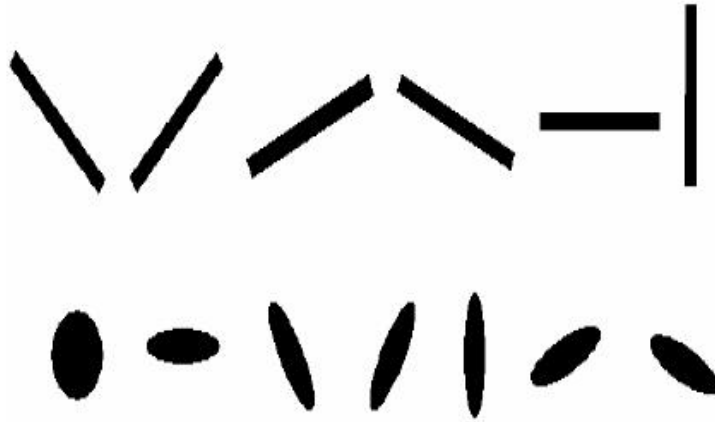


Figure 3.4: The structuring element set [27].

Park [27] proposed their morphological operator based algorithm to segment liver vessels from abdominal CT image slices. The algorithm consists of four steps. In the first step, the liver region, which is the area of interest, is segmented approximately using thresholding. In the second step, a range of structuring elements are defined based on prior knowledge. In liver vessel segmentation where the object of interest is the tubular structure, the structuring element set is made up of circle shape and stick shape with many angles, as shown in Figure 3.4. In the third step, each image slice is dilated and eroded by the structuring elements to obtain the liver vessels. In the fourth step, the 3D liver vessels are reconstructed by adding all slices together.

Morphological operation based algorithm has several advantages. First it does not need any specific initialization, which makes it possible to design the fully-automatic algorithms. Second it focuses less on the structure of the object of interest. Therefore, it can work well on the vessels whose structure varies between different persons. However, morphological operation based

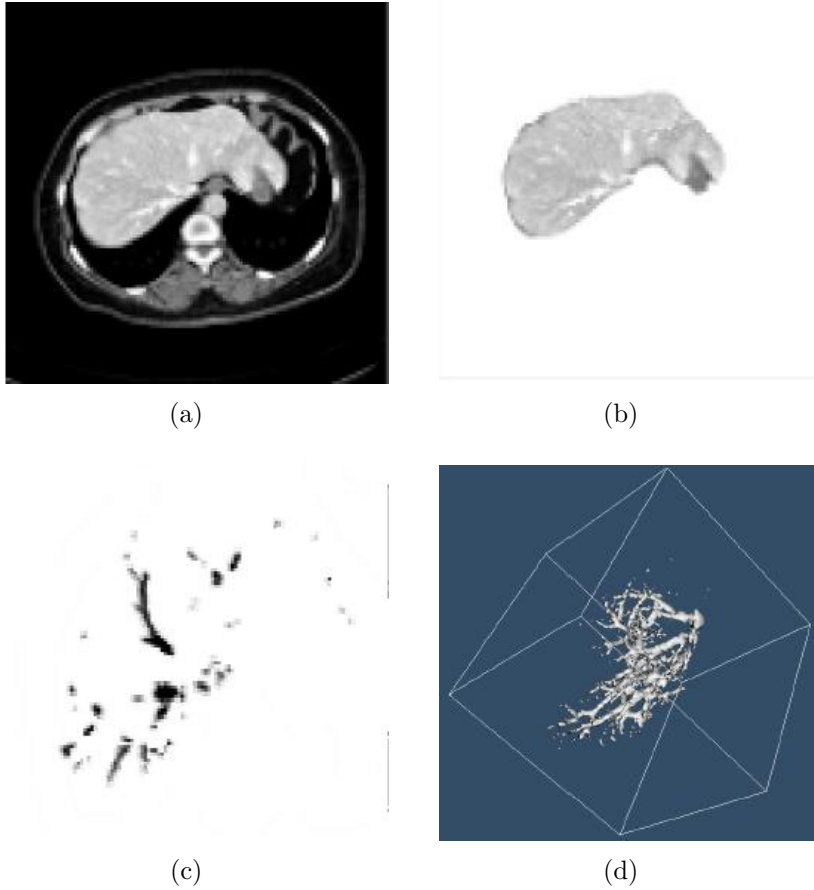


Figure 3.5: An example using morphological operation based algorithm to segment liver vessels from CT image slices [27]. (a) One CT image slice. (b) The area of interest after thresholding. (c) The segmentation result. (d) The 3D reconstruction result of the liver vessel.

algorithm is sensitive to noise. So it cannot precisely segment tiny blood vessels where noise occurs.

## 3.3 Boundary-based Approaches

### 3.3.1 Snake

Snake [15], which is also called active contour model, was first proposed by Kass, Witkin, and Terzopoulos in 1987. The snake model is represented by a series of connected points. and it can be deformed under the influence of internal forces, image forces and external forces. Internal forces are defined to constrain the stretching and banding of the snake, which keep the snake smooth throughout the deformation. Image forces are the forces derived from the image that drive the snake towards the desire feature of interest, such as the edges. External forces are the forces that constrain the deformable of the snake, which is seldom used in medical applications. Figure 3.6 shows an examples of applying snake model to segment 2D MR heart image. The snake model is initialized as a circle and then allowed to deform o the inner boundary of the left ventricle.

Snake is regarded as a good model in many medical segmentation applications. It can be deformed to any shape as long as all the forces are well defined, and it can produce a smooth and accurate boundary of the object, even if the edges of the object are disjoint in some area. However, snake also has some disadvantages. For example, It does not converge well to concave features, because the internal force of the snake can limit their geometric flex-

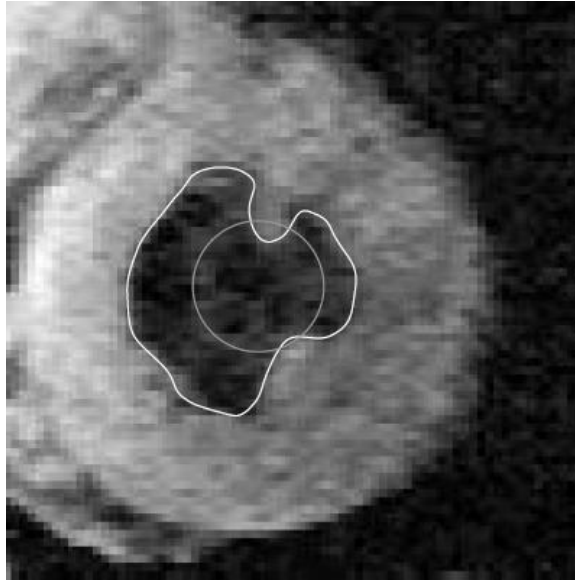


Figure 3.6: A 2D example using snake model to extract the inner wall of the left ventricle of a human heart from an MR image [29]. The snake model is initialized as a circle and then allowed to deform on the inner boundary of the left ventricle

ibility. It is also sensitive with the initialization and noise. Furthermore, the structure information must be known in advance since snake cannot segment objects with shape changes.

Several variations of snake are proposed to overcome these shortcomings. One variation is the gradient vector flow (GVF) snake [44, 42, 43] proposed by Xu and Prince. GVF field is a vector field derived from the diffusion of the gradient vectors of a gray-level or binary edge map generated from the input image. Then GVF snake uses the GVF field as the image force, which is different from the original snake that use edge map as the image force. GVF can attract the snake to fit the concave part of the object in the image. As is shown in Figure 3.7, GVF snake is less sensitive to the initialization and can segment concave object. However, it is still sensitive to the noise.

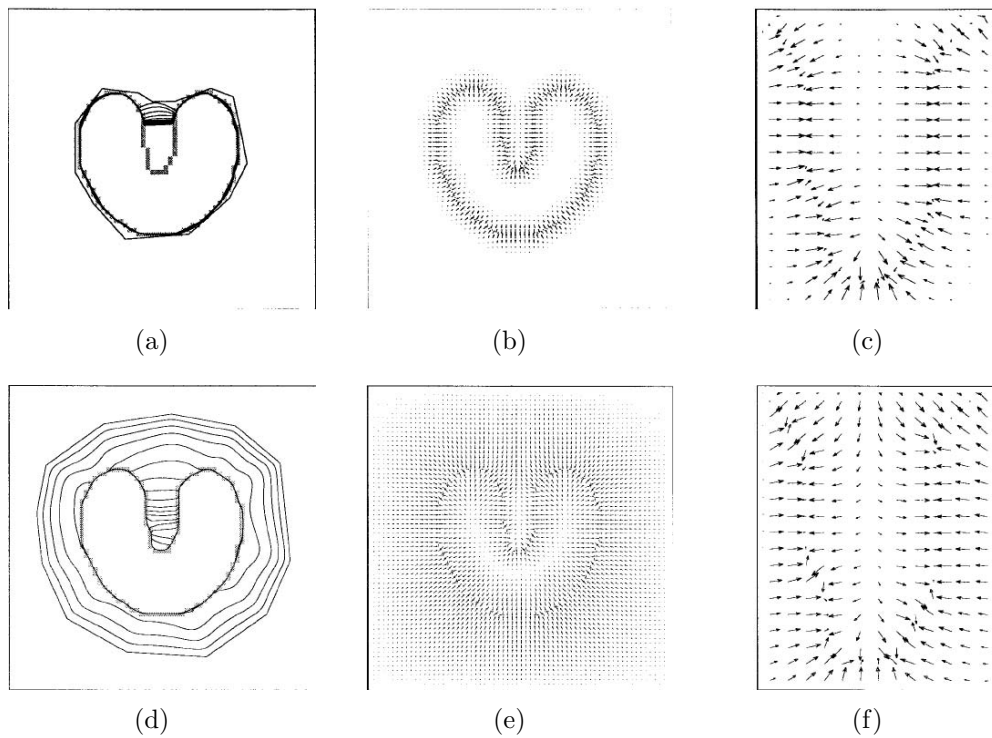


Figure 3.7: A comparison between original snake and GVF snake [42]. (a) Convergence of a traditional snake. (b) image force of the original snake (c) close-up of the concave part. (d) Convergence of a GVF snake. (e) GVF snake image forces. (f) Close-up of the concave part of GVF.

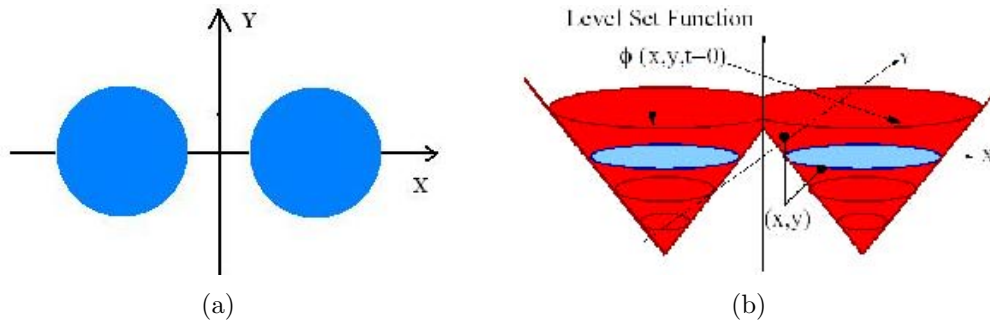


Figure 3.8: Level set. (a) A 2D contour. (b) The level set surface (red). The zero level set (blue).

Snakes can also be extended to 3D, which is referred to as the active surface. Usually a 3D surface is represented by a set of correlated control points, such as the surface mesh. External force, internal force and image force can be defined similarly as they are in 2D snake. However, due to the large amount of control points, 3D snake is reported as time-consuming.

### 3.3.2 Level Set

Level set methods [35, 33, 34] is proposed by Sethian and Osher in 1988. It solves the segmentation problem in one higher dimension.

Let  $\Gamma$  denote a closed curve in 2D. Then a level set function  $d = \phi(x(t), y(t), t)$  is defined (The red curve in Figure 3.8) to represent the distance  $d$  of the point  $(x, y)$  from  $\Gamma$ .  $d$  is positive if the point  $(x, y)$  is outside  $\Gamma$ ,  $d$  is negative if the point  $(x, y)$  is inside  $\Gamma$ , and  $d$  is zero if the point  $(x, y)$  is on  $\Gamma$ . The intersection of  $\phi(x(t), y(t), t)$  and the  $xy$  plane (the blue circle in Figure 3.8) gives the contour of  $\Gamma$ . Therefore, the contour  $\Gamma$  can be obtained by solving equation  $\phi(x(t=0), y(t=0), t=0) = 0$ , which is referred to as the zero level set.

The level set method works as follows. In the initialization step, an initial shape of  $\Gamma$  is given by the initial contour of  $\phi(x, y, t = 0)$ . After that the level set function  $\phi(x, y, t)$  moves up and down along the  $\phi$  axis under a pre-defined force  $F$ . The force is usually made up of a constant inflation term, an internal force based on the curvature of the zero level set, an image force based on the image information such as edges. This force gives the propagation speed of  $\Gamma$  in its normal direction. Numerical methods can be applied to approximate the equations of motion by computing  $\phi(x, y, t + \Delta t) = 0$  given  $\phi(x, y, t) = 0$ , where  $\Delta t$  is the time step. This evolution will iterate until the level set function converges.

Level set method is applied in many vasculature segmentation applications [20, 32]. Figure 3.9 [32] shows an example of using level set to segment arteries. The contour starts from a circle inside the blood vessel and propagates to fit the boundary of the arteries. Level set method can also be extended from 2D to 3D [41, 19, 26, 12]. For example, Magee [19] uses triangular-mesh model and 3D level set method to segment abdominal aortic aneurysms (See Figure 3.10), and Grunerbl [12] uses 3D level set method and geodesic contour to segment Femur from a range of CT slices.

The advantage of the level set method is that the level set method makes it very easy to follow shapes that change topology, for example when a shape splits into two, develops holes, or the reverse of these operations. Also, the intrinsic geometric properties of the contour can be easily determined from level set function. Level set can be easily extended to segment objects in higher-dimensional data, where the formulation is the same for higher-dimensional propagating hyper-surfaces. However original level set method

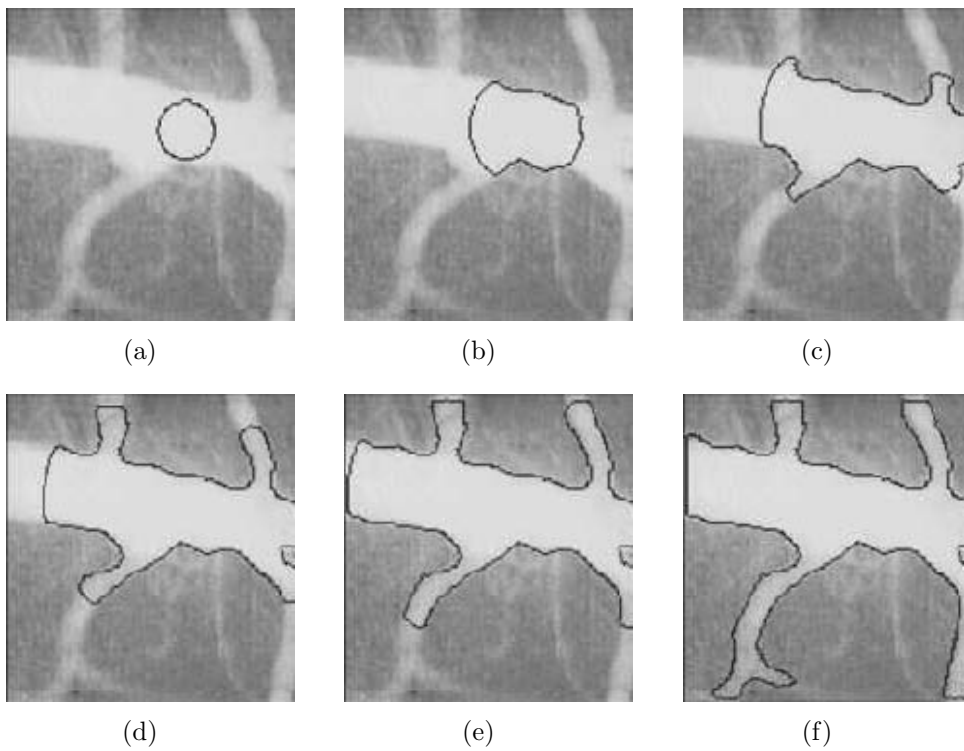


Figure 3.9: Arteries segmentation using level set method [32]. (a) The initial contour. (b-e) The contour expands to fit the contour of arteries. (f) The segmentation result.

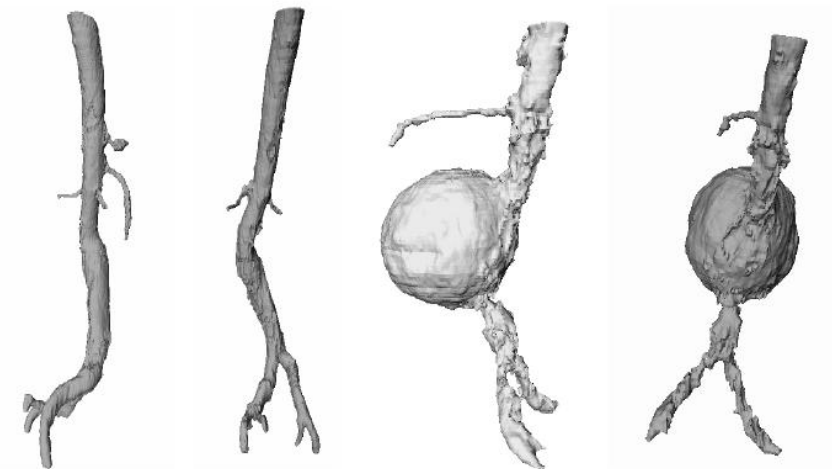


Figure 3.10: Segmentation of abdominal aortic aneurysms using 3D level set [19].

does not have any geometrical constraints. Therefore the level set may leak into some undesired regions when the input image data is not clear enough. To overcome the leakage problem, Nain [21] proposed a vessel segmentation method combining the level-set model with a soft shape prior, which is referred to as the shape driven flow. Figure shows the segmentation result using shape driven flow. As can be seen, in the areas where the image information is ambiguous, the algorithm overcomes the leakage problem.

The general level set method is also reported as time-consuming, because in each iteration the  $\phi$  value of each pixel should be re-computed. Some improvement have been done to increase the algorithm efficiency, such as the narrow band [1] and fast marching [36]. Narrow band method only updated the  $\phi$  value at a thin region around the propagating contour, because the pixels far away from the contour do not affect the propagation. Fast marching method is very efficient for the case in which the contour is always

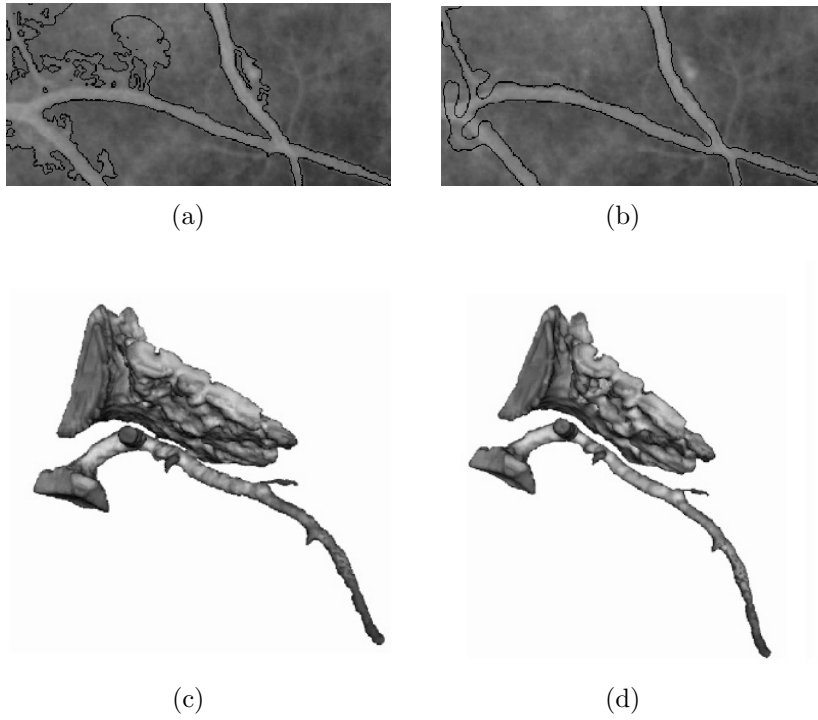


Figure 3.11: A comparison of the level set segmentation algorithm with and without shape driven flow [21]. (a) 2D segmentation result without shape driven flow. (b) 2D segmentation result with shape driven flow. (c) 3D segmentation result without shape driven flow. (d) 3D segmentation result with shape driven flow.

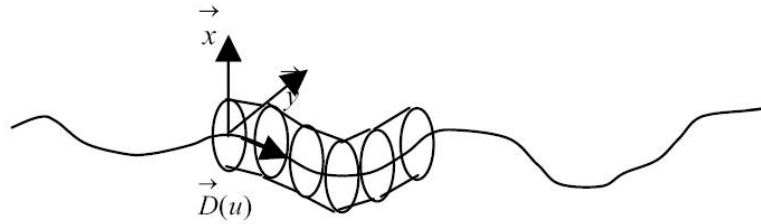


Figure 3.12: A typical parametric model of blood vessel [7].

propagating in the same direction at a particular speed.

### 3.3.3 Parametric Model-based Approaches

Parametric model based approaches define objects perimetrically. In vascular structure segmentation applications where blood vessels are tube-like objects, blood vessels are defined as a set of overlapping ellipsoids. After that, the initial model is deformed and aligned to each 2D slice of a 3D volumetric data to get a best fit.

Generally, the parametric model consists of a space curve, or axis, and a cross-section function defined on the axis [18]. In blood vessel segmentation area, the blood vessels are cylindrical shape, so the cross-section function is usually an ellipse. Therefore, the blood vessels are defined by a cross-sectional element that is swept along the axis using some sweep rules. (See Figure 3.12)

Pellot [28] used parametric model based method to segment blood vessels with concentric stenoses from two-view XRAs. Their model are initialized using a stack of parallel 2D ellipses (See Figure 3.13) and then the initial model is deformed to fit the two-view XRA images. An adaptive simulated

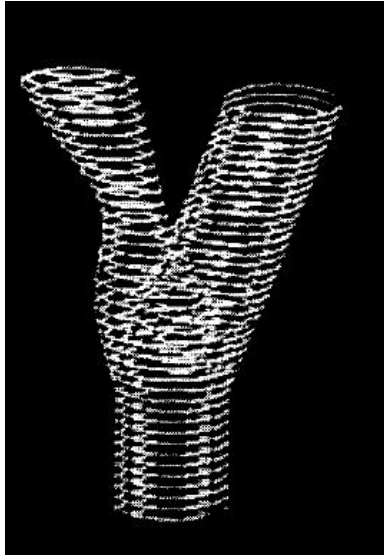
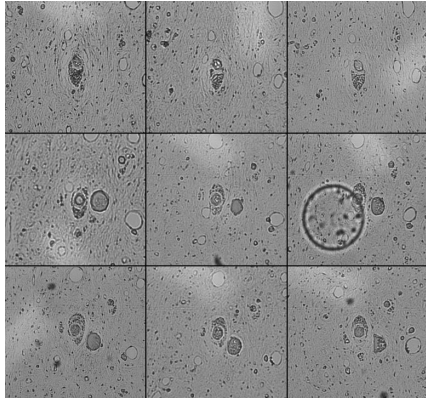


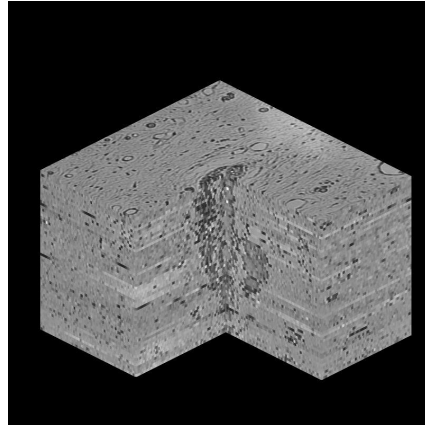
Figure 3.13: A blood vessel model using a stack of parallel 2D ellipses [28].

annealing optimization algorithm is used to control the deformation. Properties on the optimal solution are described by a Markov Random Field. The method is reported to perform well both on single vessels and on branches.

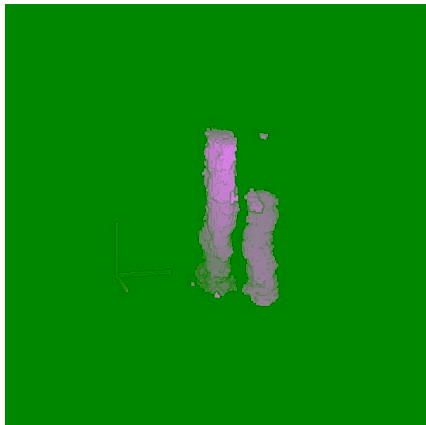
Bors [4] uses geometric model to segment tooth pulpal blood vessel from image volume data. In their approach, the object is considered as a stack of overlapping ellipsoids whose parameters are found using the normalized first and second order moments. The segmentation process is based on the geometrical model and gray-level statistics of the images. It consists of two steps. In the first step, the center of the ellipsoids are estimated using an extended Hough Transform algorithm in 3D space. Then a Radial Basis Function (RBF) network classifier is employed to model the 3D structure and gray-level statistics. In their RBF classifier, each unit corresponds to an ellipsoid. The learning of the RBF network is based on the  $\alpha$ -Trimmed Mean algorithm.



(a)



(b)



(c)



(d)

Figure 3.14: Segmentation of tooth pulpal blood vessel using geometric model [4]. (a) The input image slices. (b) 3D visualization of the stack of frames. (c) The segmentation result using RBF algorithm. (d) Segmentation result using  $\alpha$ -Trimmed Mean RBF algorithm.

O'Donnell [24, 25] use a form of geometric cylinder model to segment cylindrical structures from CT angiogram. The model is initialized as a volume created by cross-section swept along a 3D curve, which is regarded as the centerline. The centerline is represented by a 3D cubic B-spline and the cross-section swept is always in the plane orthogonal to the centerline to form the cylinder. The strength of the model comes from additional finite element (FEM) mesh-like component lying on top of their model to address the fine detail in complex structures. In order to insure a smoothness of fit, this mesh-like component is endowed with a stretching penalty which penalizes sharp edges. Figure 3.15 represents the segmentation result of the aortic arc from CT angiogram.

Parametric model based approaches have a lot of advantage. They can guarantee the smoothness and robustness of the reconstructed tubular surface. Also, parametric model based approaches do not have leakage problems, because the shape is preserved in the segmentation procedure. However, parametric model based approaches has three limitations. First, it makes the assumption that the vasculature should be tube-like object. Therefore, they can only segment some parts of the vasculature where this assumption holds. Second, parametric model based approaches are sensitive to the initialization. If not initialized properly, parametric model based approaches may fail in some cases where the vascular structures are very complex. Third, parametric model based approaches requires large quantities of computation, which makes it very slow where the blood vessel structure is complex.

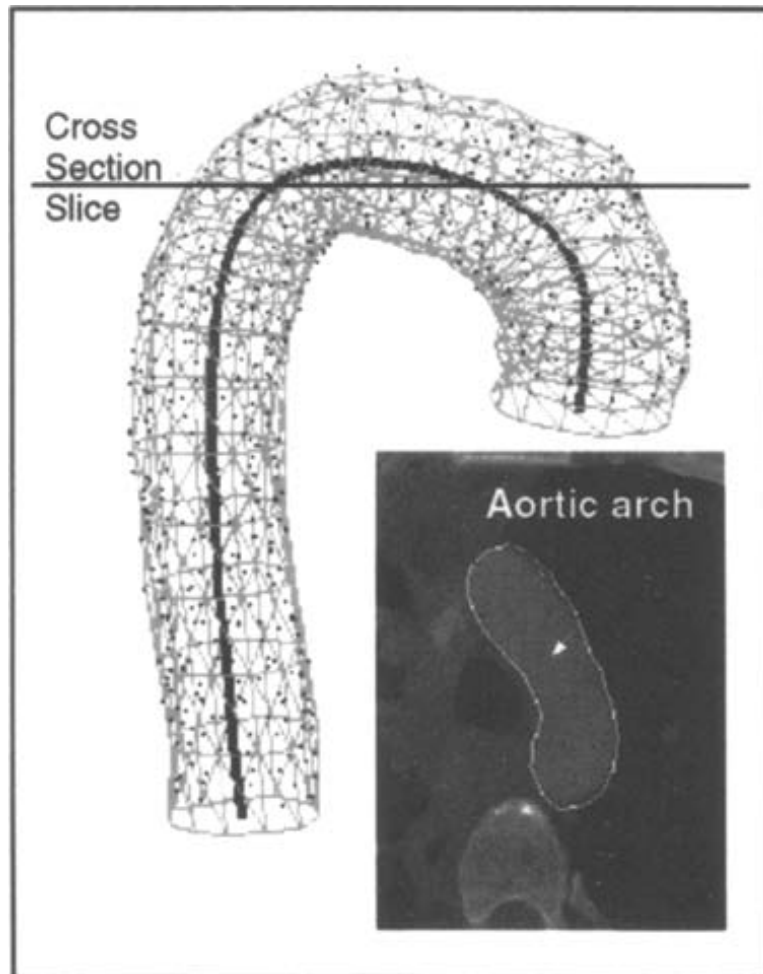


Figure 3.15: The final result of O'Donnell's model to segmented a healthy human aortic arch from spiral CT angiogram data. [25]

### 3.4 Summary

In this section current segmentation algorithms on blood vessel segmentation are reviewed, including centerline-based approaches, region-growing approaches, morphology-based approaches, snakes, level-set and parametric model-based approaches. Pros and cons are also analyzed.

Centerline based approaches perform well in maintaining complex vascular structure, and do not need specific initialization, but they are sensitive to noise, which makes it impossible to segment tiny blood vessels where noise occurs. So in hepatic vein segmentation, pure centerline based approaches will overlook some tiny hepatic vein branches due to noise.

Region growing based approaches can correctly segment regions that have the same properties and are spatially separated. However, in hepatic vein segmentation, it is very hard to define the grouping homogeneity criteria. Moreover, there is a lot of noise in liver CT images, which may cause serious leakage problem. Therefore, region growing based approaches are not applicable in hepatic vein segmentation.

Morphological operation based approaches are not sensitive to the initialization, and they focus on not the tree structure of the object but the object shape. Therefore, it cannot produce accurate result.

Snake is deformable model based approach, which can be deformed to any shape as long as all the forces are well defined, and it can produce a smooth and accurate boundary of the object, even if the edges of the object are disjoint in some area. However, snake cannot handle structure change during the segmentation procedure. In hepatic vein segmentation, the structure of

the hepatic vein is unknown, so the initialization of the snake will be very specific and complex. Therefore, snake is not applicable in hepatic vein segmentation.

Level set method can easily segment objects with topology change. And it do not need any specific initialization. The intrinsic geometric properties of the contour can be easily determined from level set function. However, in hepatic vein segmentation, the blood vessel boundaries in CT images are not so clear, and the blood vessels have narrow diameter in some area. As a result, the initial contour (or 3D surface) cannot propagate to fit the boundary of the hepatic vein precisely. In some area the contour may stop propagating due to the narrow vessel, and in some area the contour may leak out due to the fuzzy vessel boundary. So some modification should be applied on level set method to overcome these drawbacks..

Parametric model based approaches define the initial blood vessel model parametrically, and then deform the model to fit the image data. They can produce a smooth and robust 3D blood vessel segmentation result. However, they require large amount of user input, especially when segmenting tree-structured blood vessels.

## Chapter 4

# Fast Marching Method Driven by Gaussian Mixture Models

Segmentation of tree-structured blood vessel in CT image slices is a crucial step in medical diagnosis and surgery. The related work reviewed in Chapter 3 shows that this problem has not been well solved. Existing algorithms can perform fairly in single branch blood vessel segmentation. However, they cannot work well on tree-structured blood vessel with many branches. For example, centerline based approaches require a large amount of user input to segment each branch separately, region-based approaches are not robust enough, and parametric-model-based algorithm are slow and sensitive to the initialization. The major contribution of this research is developing a fast and accurate semi-automatic blood vessel segmentation algorithm which requires a small amount of user inputs and is easy to use.

## 4.1 Problem Description

### 4.1.1 Input Data

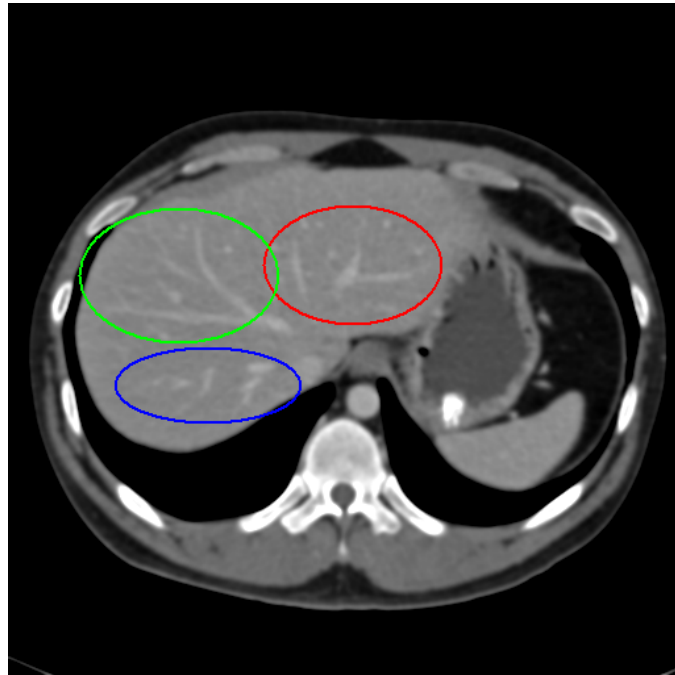
The input data of this project are liver CT images collected from National University Hospital. In our experiment, every data set is made up of about 320 slices, and the size of each CT slice is  $512 \times 512$  pixels. The inter-slice thickness is 1.0mm.

Figure 4.1(a) represents the main branches of hepatic vein in data set 1. As can be seen, there are six main branches in this data set. The white area in the blue circle is the right hepatic vein, the two vessel in the green area is the middle hepatic vein, while the three vessels in the red circle is the right hepatic vein. Figure 4.1(b) represents the main branches of hepatic vein in data set 2. The left, middle and right hepatic veins are also labels with blue, green and red correspondingly.

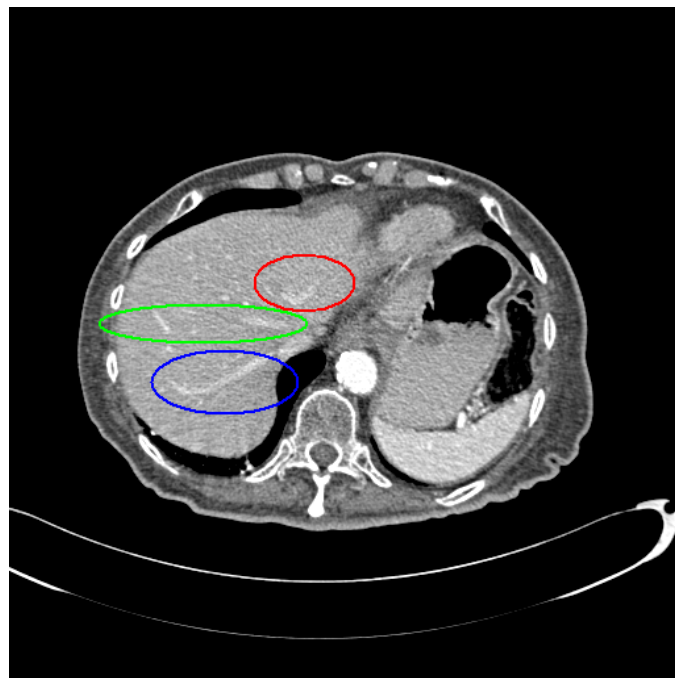
However, compared with data set 1, data set 2 has fewer branches. As can be seen, there are only one branch in the middle hepatic vein, and only two branches in the right hepatic vein. This diversity is very common between human beings. Our algorithm is capable to segment all types of hepatic vein without special initialization.

### 4.1.2 Overview of Algorithms

According to the characteristic of the hepatic veins, fast marching is selected as the main segmentation method in my algorithm. Gaussian mixture model (GMM) is chosen to determine the propagating speed during the propagation



(a)



(b)

Figure 4.1: The diversity of hepatic vein between patients. The vessel ladled with blue, green and red are left, middle and right hepatic vein correspondingly. Data collected from National University Hospital, Singapore.

procedure. Parametric-cylinder-model is selected to segment the vena cava and remove it from the segmentation result. In general, our hepatic vein segmentation algorithm consists of three steps as follows:

- Noise Removal of CT data
- Hepatic vein segmentation using fast marching method
- Vena cava removal using cylinder-model-based method

The flow of the algorithm is shown in Figure 4.2.

## 4.2 Hepatic Vein Segmentation Algorithm

### 4.2.1 Noise Removal

Noise in CT images has many origins. Generally they can be categorized into two groups: The noise caused by human body motion and the noise caused by X-ray CT technique.

Human body motion during the imaging procedure may cause the misalignment between CT slices. A global registration algorithm can remove this kind of noise well. In my experiment data, the patient kept still during the imaging procedure, so it is not necessary to align all CT slices before segmentation.

The noise caused by CT techniques is called quantum noise. This kind of noise is caused by the radioactive source itself, which is unavoidable in CT images. The higher the image resolution is, the more this noise occurs. In our experiment, the resolution in each CT slice is between 0.63mm and

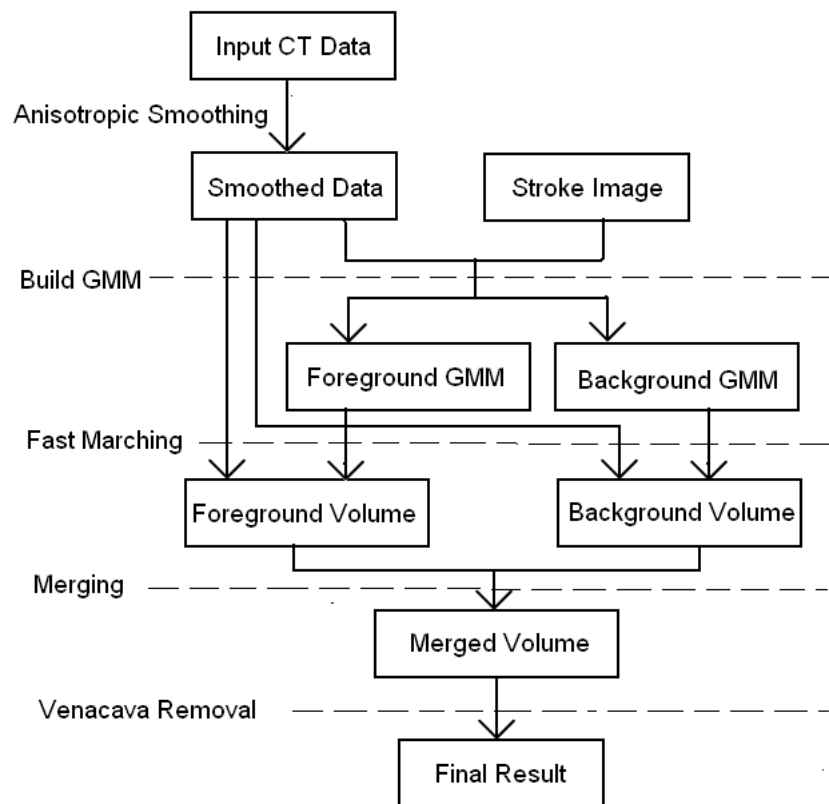


Figure 4.2: The flow of my algorithm.

0.74mm per pixel and the inter-slice thickness is 1.0mm, and this kind of noise cannot be overlooked in the experiment. Therefore, a noise removal procedure should be applied before segmentation.

In my experiment, anisotropic diffusion is selected as the smoothing filter. Anisotropic diffusion is a non-linear smoothing filter, which is the solution to the heat equation, with a variable conductance term to limit smoothing at edges. The kernel equation is given as follows.

$$\frac{\partial I(\mathbf{x})}{\partial t} = \nabla C(\mathbf{x}) \cdot \nabla I(\mathbf{x}) + C\Delta I(\mathbf{x}) \quad (4.1)$$

where  $I(\mathbf{x})$  denotes the pixel value at location  $\mathbf{x}$ ,  $C(\mathbf{x})$  denotes the conductance value at location  $\mathbf{x}$ .  $\nabla$  is the gradient, and  $\Delta$  is the Laplacian operator. The variable conductance term  $C(\mathbf{x})$  is given by

$$C(\mathbf{x}) = e^{-\left(\frac{\|\nabla I(\mathbf{x})\|}{K}\right)^2} \quad (4.2)$$

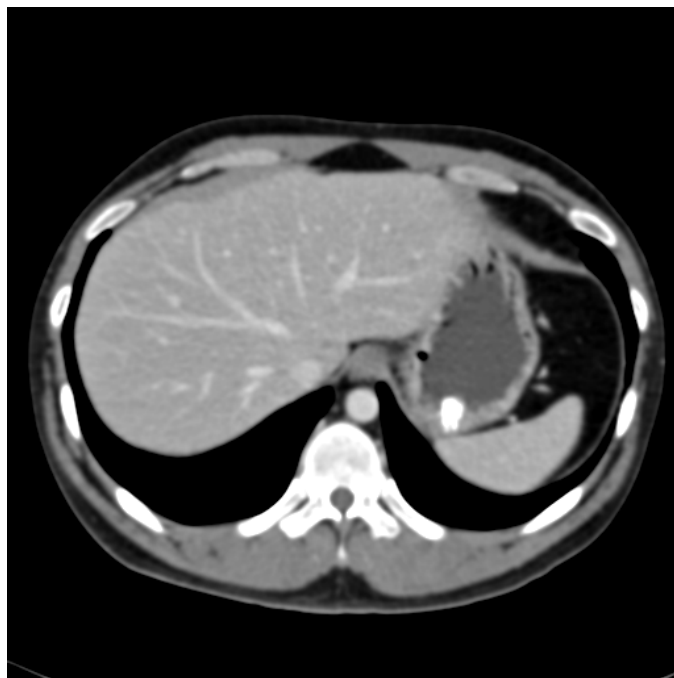
here the constant  $K$  controls the sensitivity to edges and is chosen experimentally. In my experiment  $K = 0.25$ . Figure 4.3 represents the noise removal result using anisotropic smoothing filter. As can be seen, the quantum noise is removed significantly, and the boundary of the hepatic vein is preserved.

## 4.2.2 Hepatic Vein Segmentation Using Fast Matching Method

Fast marching method is introduced by James A. Sethian as a numerical method for solving boundary value problems. Typically, such a problem



(a)



(b)

Figure 4.3: Noise removal using anisotropic smoothing filter. (a) The original CT slice. (b) The noise removal result.

describes the evolution of a closed curve (or a surface in 3D) as a function of time  $T$  with speed  $F(\mathbf{x})$  in the normal direction at a point  $\mathbf{x}$  on the curve (or a surface in 3D). The force  $F$  is always be positive, such that the curve (or surface in 3D) can only propagate outward. If the force is large, the cost time for the point arriving the next position is small. If the force is small, the cost time for the point arriving the next position will be large. If the force equals 0, the cost time will be infinite, and the propagation stops.

The definition of the force  $F$  varies in different applications. In my algorithm, the force is calculated using Gaussian mixture model.

In the first step, one CT slice that containing the hepatic vein is selected, and some strokes are marked to identify the hepatic vein area and non-hepatic vein area. Figure 4.4 is an example of stroke image in my algorithm. The red lines denotes the hepatic vein area, and the green lines denotes all non-hepatic vein area.

After that the pixel values on the red strokes and green strokes are obtained from CT data. Histograms for the hepatic vein area and non-hepatic vein area are build separately.

The segmentation for hepatic vein area and non-hepatic vein area are done parallely. The procedure of non-hepatic vein area segmentation is the same as that of hepatic vein area. For simplicity, here we only describe the procedure of hepatic vein area segmentation.

Figure 4.5 represents the intensity distribution of both the hepatic vein area and non-hepatic vein area. As can be seen in Figure 4.5, the intensity distribution of the hepatic vein varies from 100 to 460, and the intensity distribution of non-hepatic vein area varies from -150 to 180. Several peaks

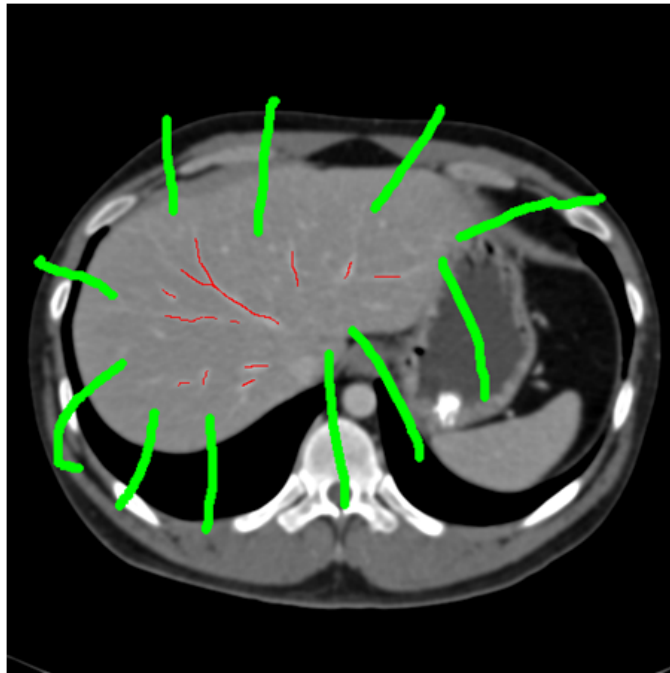


Figure 4.4: An example of the stroke image. The red strokes denotes the hepatic vein area, and all green strokes denotes the non-hepatic vein area.

can be seen in both histograms. Gaussian mixture model is selected to model the intensity distribution of the pixels. However, the number of peaks and peak values varies due to the individual differences in different data sets, so it is impossible to assign constant parameters to model the distribution. To solve this problem, we developed an adaptive binning method to assort all pixel values into different clusters automatically. The adaptive binning method works as follows.

All pixel values  $V_1, V_2, \dots, V_m$  are added into an vector and each value is picked out one by one in a random order. To each pixel value  $V_i$  that are picked out, calculate the distance  $D_{i,j}$  between  $V_i$  and the centroids of all existing clusters,  $C_1, C_2, \dots, C_n$ . Then the closest cluster is found. If the closest distance is smaller than a threshold value  $T$  (in my experiment  $T = 30$ ),  $V_i$  is added in to this cluster, and the centroid of the cluster is updated. If the closest distance is larger than  $T$ , a new cluster is generated, and  $V_i$  will be the centroid of the new cluster. After all pixel values are assigned, those clusters with less than 30 pixel values will be deleted automatically. After all clusters  $C_1, C_2, \dots, C_n$  are built, the Gaussian parameters are estimated for each cluster. Then to each value  $v$  that may occurs in the image, the probability table is built based on the formula below:

$$P(\text{Pixel}_{value} = v | \text{Pixel} \in \text{Foreground}) = \sum_{i=1}^n P(\text{Pixel} = v | \text{Pixel} \in C_i) \cdot W_i \quad (4.3)$$

where  $W_i$  is the weight of  $C_i$  given by :

$$W_i = \frac{|C_i|}{\sum_{k=1}^n |C_k|} \quad (4.4)$$

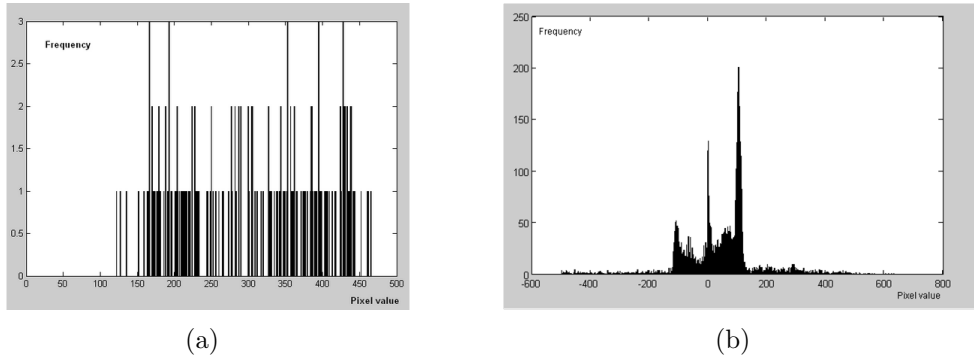


Figure 4.5: The histogram of the pixel values that are shown in Figure 4.4. (a) The histogram of hepatic vein area. (red stroke in Figure 4.4) (b) The histogram of non-hepatic vein area. (green stroke in Figure 4.4)

After that the speed function for fast marching method is assigned to each pixel based on the probability table. In the area where this pixel is more probable to be the hepatic vein area, the speed at this pixel is large. In the area where this pixel is less probable to be the hepatic vein area, the speed at this pixel is small or even equals to 0. The starting seed points are the pixels marked in the stroke image, and the stopping time is 300 in my experiment.

Figure 4.6 represents the foreground volume and background volume using fast marching method with stopping time 300. As can be seen, there are lots of overlapping between these two volumes. So a merging procedure need to be applied to obtain the hepatic vein area. Our merging criteria is as follows. Let  $FG$  denotes the To any voxel in the CT volume:

- If the voxel is in foreground volume and not in background volume, it is the hepatic vein voxel.
- If the voxel is not in foreground volume and in background volume, it

is the non-hepatic vein voxel.

- If the voxel is either in foreground volume or in background volume, it is the non-hepatic vein voxel.
- If the voxel is both in foreground volume and in background volume, compare the arriving time in fast marching procedure. If the arriving time in foreground volume is smaller, it is the hepatic vein voxel. Otherwise it is the non-hepatic vein voxel.

The merging result can be seen in Figure 4.7. As can be seen, all the branches are successfully segmented. However the undesired vena cava is also segmented in the result. This can not be avoided using fast marching method, because the hepatic vein connects with vena cave and the pixel intensity is the same in CT images. So we should use some other method to remove the vena cava.

### 4.2.3 Vena Cava Removal

As discussed in the previous section, the vena cava is also segmented using GMM-driven fast marching method, which is not a part of the hepatic vein. So an additional procedure is required to cut off vena cava from the segmentation result.

Seen from Figure 4.7, the vena cava is a straight and tubular shape object. So in my framework, parametric cylinder model based algorithm is selected to segment vena cava individually. The algorithm consists of two steps: The centerline detection and the cylinder fitting.

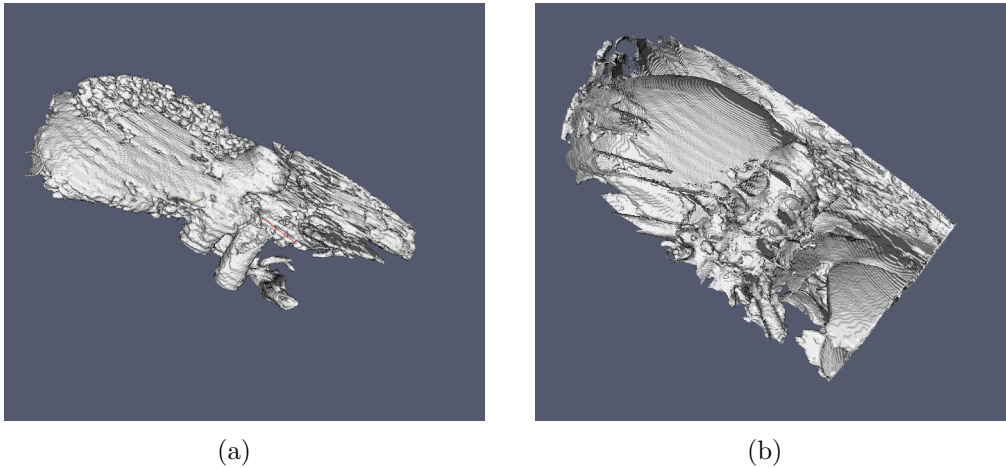


Figure 4.6: The foreground volume and background volume in hepatic vein segmentation algorithm. (a) The foreground volume with stopping time 300. (b) The background volume with stopping time 300.

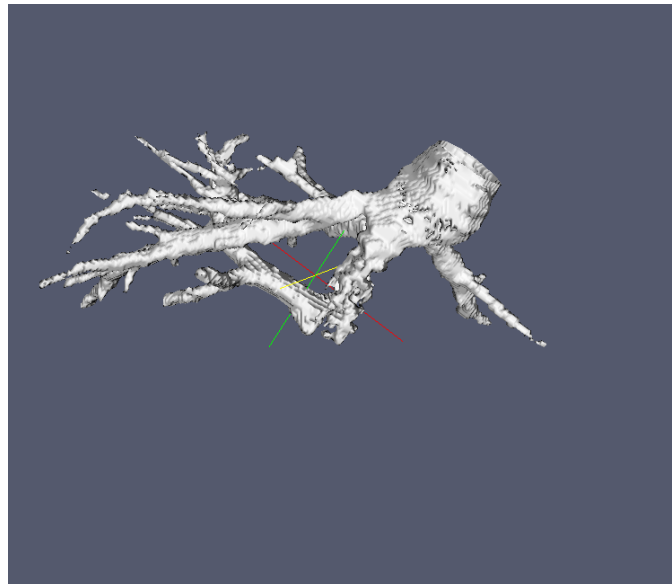


Figure 4.7: The merging result from foreground volume and background volume shown in Figure 4.6

## Centerline Detection

Centerline detection algorithms are designed to find the centerlines of the entire blood vessel. It is based on the assumption that the centerlines are the brightest lines along the blood vessels. In my algorithm, the centerline detection method proposed by [30] is applied.

Given the begin point  $V_0$  and end point  $V_n$  in an image  $I$ , the algorithm can automatically find a series of adjacent points  $v_1, v_2, \dots, v_{n-1}$  that minimize the cost function

$$Cost = \sum_{k=0}^{n-1} (w_1(1 - I_k)) + w_2 \cdot d(k, k + 1) \quad (4.5)$$

The first term of the cost function is the intensity cost.  $I_k$  is the normalized image intensity at point  $v_k$ . The second term is the distance cost, representing the distance between points  $v_k$  and  $v_{k+1}$ .  $w_1$  is the intensity weight and  $w_2$  is the distance weight.

After the centerline is obtained, the centerline is resampled and smoothed using B-spline interpolation.

## Cylinder Fitting

The parametric cylinder model represents a tubular shape object as a series of  $n$  connecting cylinders. Each cylinder consists of 4 parameters: the centerline location  $(x, y, z)$  and the radius  $r$ . The parameters of the cylinder model are estimated by minimizing the cost function

$$Cost = \sum_{k=1}^{k=n-1} (w_1 \cdot C_i(k) + w_2 \cdot C_r(k) + w_3 \cdot C_d(k)) \quad (4.6)$$

This cost function is similar with the cost function in [30]. However here we use global cylinder fitting instead of local sphere fitting in [30].

The first term  $C_i(k)$  is the intensity. It aims at finding an optimal cylinder between centerline pint  $P_k$  and  $P_{k+1}$  that can classify the voxels into two groups with minimum intensity difference. In practice, the definition of  $C_i(k)$  is given by

$$C_i(k) = \sum_{d(P', P_k, P_{k+1}) < r} |I(P') - I_{in}| + \sum_{r < d(P'', P_k, P_{k+1}) < 2r} |I(P'') - I_{out}| \quad (4.7)$$

where  $d(P', P_k, P_{k+1})$  represent the point-line distance between point  $P'$  and line  $(P_k, P_{k+1})$ .  $I_{in}$  is the average intensity of voxels in vena cava area, and  $I_{out}$  is the average intensity of voxels outside vena cava. There two parameters are given by experience.

The second term  $C_r(k)$  is the radius cost. It is defined by

$$C_r(k) = |r(k+1) - r(k)| \quad (4.8)$$

It reveals that the radius should not change too much between adjacent cylinders.

The third term is the distance constrain. The center of the cylinder should be as close as the corresponding centerline point obtained in the previous step. So this term is defined by

$$C_d(k) = d(P_k, P_{k0}) \quad (4.9)$$

The final cost function is the combination of there three terms with

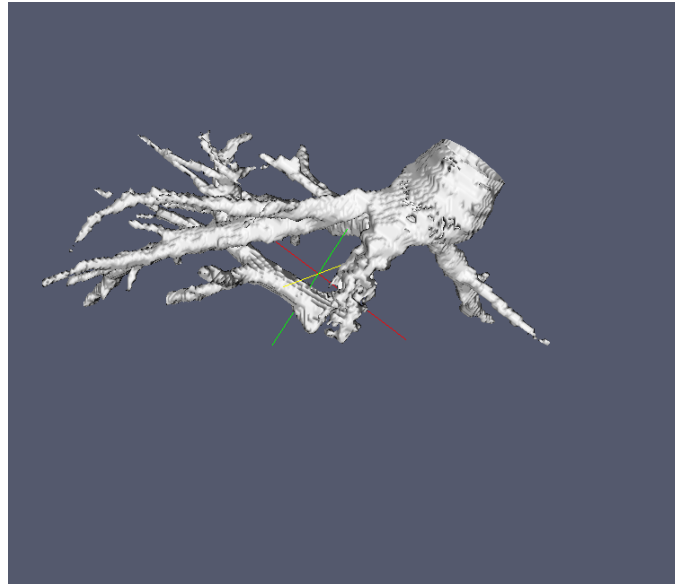
weights that are given in 4.6.  $w_1$ ,  $w_2$  and  $w_3$  are the weights defined by users. The parameters are estimated using Insight Toolkit. The segmented vena cava are deleted from the hepatic vein.

Figure 4.8 shows the segmented hepatic vein after vena cava removal. As can be seen, the undesired vena cava is successfully removed from the hepatic vein.

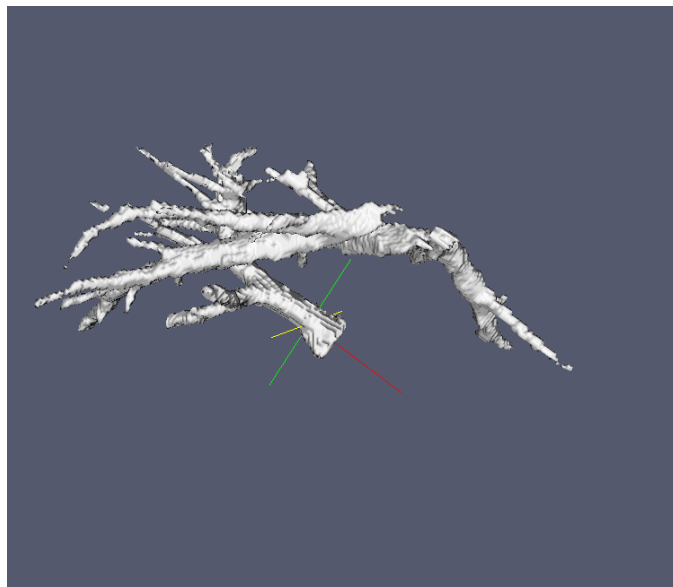
### 4.3 Performance Measure

As a comparison, region growing method is applied to the same data set. Figure 4.9 shows the comparison between region growing result and my result. As can be seen, region growing methods as serious leakage problem. Its result includes not only the hepatic vein but also the portal vein and vena cava. So it is not applicable in hepatic vein segmentation area.

Level-set algorithm is a state-of-art parametric segmentation algorithm which is widely applied in medical image segmentations. So in my experiment, level-set algorithm is also applied to the same data set as a comparison. The level-set algorithm in my experiment is implemented by ITK-SNAP. As can be seen in Figure 4.10, the level-set algorithm with low smooth constrain has a serious leakage problem. The segmentation result leak to the liver tissue and abdominal muscle area. Figure 4.11 is the segmentation result using level-set algorithm with high smooth constrain. As can be seen in Figure 4.11, the propagating surface cannot reach to the end part of the blood vessel. That is because the smooth constraint keeps the shape and prevents the surface to propagate outwards. Figure 4.12 is the segmentation result

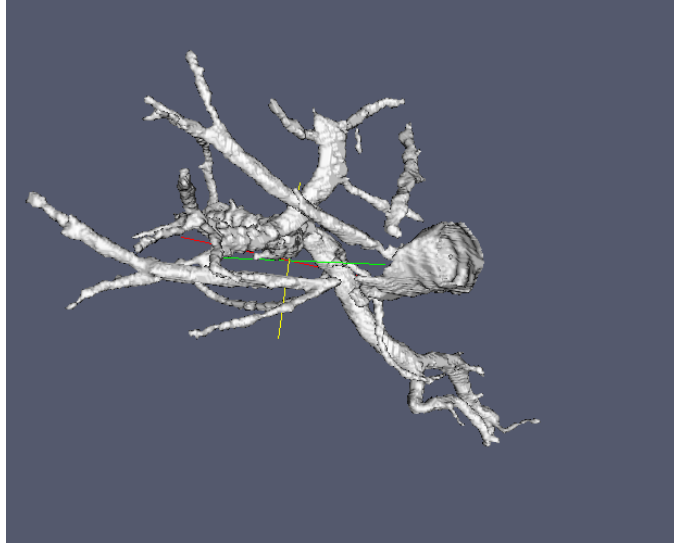


(a)

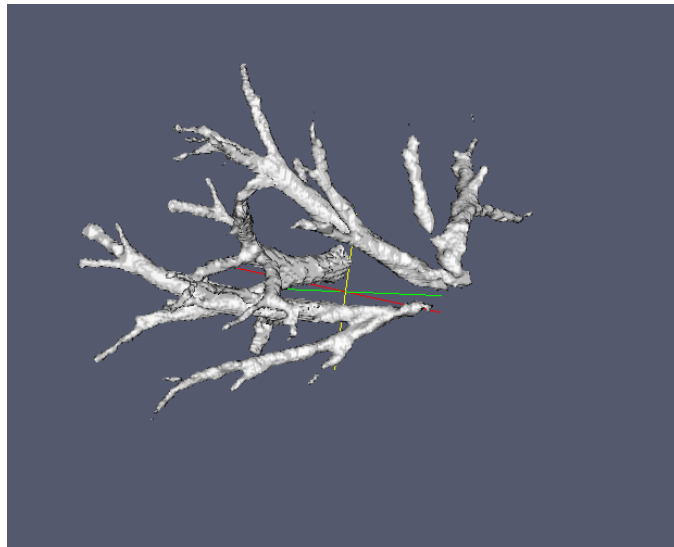


(b)

Figure 4.8: The vena cava removal result. (a) The hepatic vein before vena cava removal. (b) The hepatic vein after vena cava removal.



(a)



(b)

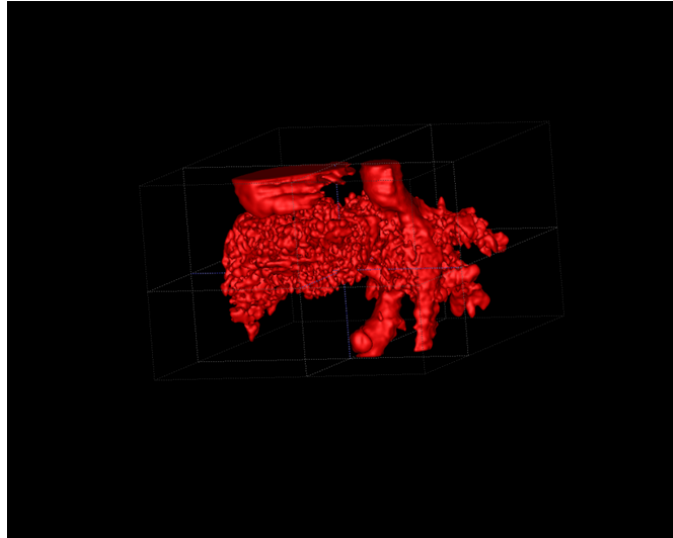
Figure 4.9: The comparison between region growing and my result. (a) The region growing result. (b) My result.

Table 4.1: The cost time comparison between my algorithm and existing algorithms)

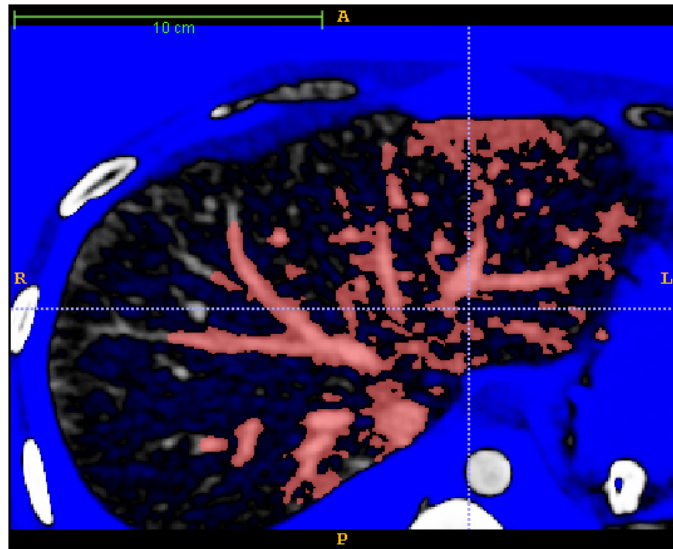
	Cost Time	Drawback
My algorithm	115 seconds	Overlook some tiny bifurcate branches
Region growing	47 seconds	Serious leakage
Levelset with low smooth constrain	337 seconds	leakage
Level Set with high smooth constrain	291 seconds	Cannot reach the end part of hepatic vein branches

of my algorithm at the same slice. Compared with level-set algorithm, my algorithm produces a much better result.

The efficiency is also compared between my algorithm, level-set algorithm and region growing. Table 4.1 represent the time cost of each algorithm. The time is recorded in my desktop PC (2G memory and 2.3GHz CPU). As can be seen, my algorithm is 2-3 times faster than level-set algorithm. Region growing algorithm is faster than my algorithm, but it cannot overcome serious leakage problem and cannot produce satisfactory result.

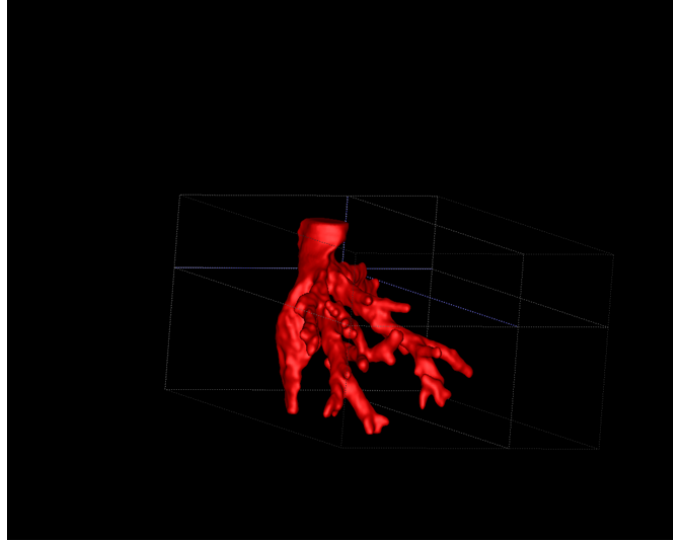


(a)

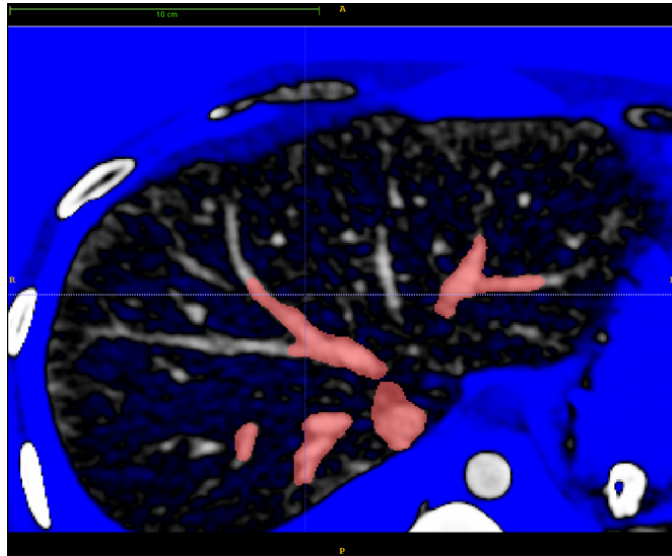


(b)

Figure 4.10: The segmentation result using level-set with low smooth constrain. (a) The 3D segmentation result. (b) The cross-section between one image slice and the segmentation result.

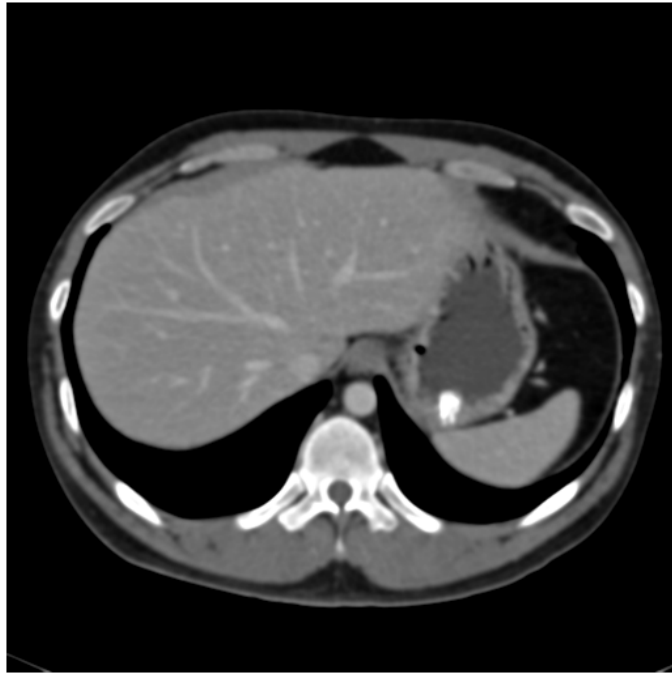


(a)

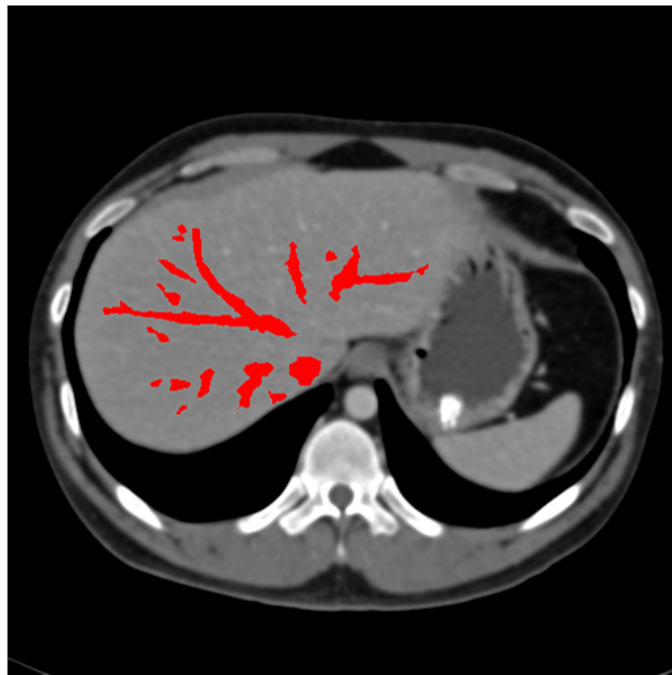


(b)

Figure 4.11: The segmentation result using level-set with high smooth constrain. (a) The 3D segmentation result. (b) The cross-section between one image slice and the segmentation result.



(a)



(b)

Figure 4.12: The segmentation result of my result. (a) A selected image slice. (b) My segmentation result.

# Chapter 5

## Conclusion and Future Work

Blood vessel segmentation is a crucial step in medical diagnose and diagnosis. In this thesis, existing blood vessel segmentation algorithms are reviewed. The literature review shows that none of current algorithms can segment hepatic vein in CT images well.

This thesis describes the segmentation algorithm on hepatic vein in CT images. First, anisotropic filter is applied on CT data to remove noise. After that, Gaussian mixture models are build for both hepatic vein area and non-hepatic vein area based on a stroke image drawn by the user. Then the fast marching algorithm are run in parallel on the same data set. An first-come-first occupy criteria is set in the merging procedure to solve the leakage problem. Finally the vena cava are segmented and removed from the hepatic vein using parametric cylinder model based segmentation.

The main contribution of my thesis is that I develop an algorithm to segmented the tree-structured hepatic veins from CT images. My algorithm satisfies all the objectives proposed in Chapter 1.2. As discussed in Chapter 4,

my algorithm can successfully segment the main branches as well as bifurcate branches of the hepatic vein. My algorithm can also remove vena-cava from the segmentation result, which may be wrongly segmented by some other algorithms such as level-set. The output of my algorithm is the 3D volumetric model of hepatic vein, and the segmentation result is verified by doctors in National University Hospital. The location, orientation and thickness of the hepatic vein is accurate enough for liver transplanting operation. My algorithm is efficient and effective. In real applications my algorithm requires only about 115 seconds to obtain the volumetric hepatic vein model. My algorithm requires little amount of user input. The doctors only require several seconds to draw several simple strokes in one selective images and mark the begin and end points of the vena cava.

A comparison between my algorithm and existing algorithms is also given. Region growing and level-set are selected as a comparison because they are two state-of-art algorithms that are widely applied in medical image segmentation applications. My algorithm requires 115 seconds to obtain the result. The main branches are successfully segmented and the vena-cava is removed. Only some unimportant bifurcated branches are missed. Region growing is 3 times faster than my algorithm, however it has serious leakage problem. Level-set algorithm is much slower than my algorithm. Level-set with high smooth constrain cannot reach the end part of hepatic vein, while level-set with low smooth constrain has leakage problem.

My algorithm still has some limitations. For example, it may overlook some tiny bifurcate branches with radius smaller than 1 pixel size. In future, some further knowledge, e.g., the location and shape of liver organ and portal

vein, may be interpolated to solve this problem.

# Bibliography

- [1] D. Adalsteinsson and J. Sethian. A fast level set method for propagating interfaces. *Journal of Computational Physics*, 118:269–277, 1995.
- [2] S. Aylward and E. Bullitt. Initialization, noise, singularities, and scale in height ridge traversal for tubular object centerline extraction. *IEEE Transactions on Medical Image*, 21(2):61–75, Feb 2002.
- [3] S. Aylward, S. Pizer, S. Bullitt, and D Eberl. Intensity ridge and widths for tubular object segmentation and description. In *In Proceedings of the Workshop on Mathematical Methods in Biomedical Image Analysis*, pages 131–138, 1996.
- [4] A. Bors and I. Pitas. Object segmentation and modeling in volumetric images. In *In Proceedings of Workshop on Non-Linear Model Based Image Analysis*, pages 295–300, 1998.
- [5] K. Chandrinos, M. Pilu, R. Fisher, and P. Trahanias. Image processing techniques for the quantification of atherosclerotic changes. In *In Proceedings of the Mediterranean Conference on Medical and Biological Engineering and Computing*, 1998.
- [6] S. Eiho and Y. Qian. Detection of coronary artery tree using morphological operator. *IEEE Computational Cardiology*, 24:525–528, 1997.

- [7] J. Feng, H. Ip, and S. Cheng. A 3D geometric deformable model for tubular structure segmentation. In *In Proceedings of Multimedia Modelling Conference*, pages 174–180, 2004.
- [8] M. Figueiredo and J. Leitaó. A nonsmoothing approach to the estimation of vessel contours in angiograms. *IEEE Transactions on Medical Image*, 14:162–172, 1995.
- [9] C. Florin, R. Moreau-Gobard, and J. Williams. Automatic heart peripheral vessels segmentation based on a normal mip ray casting technique. In *In Proceedings of International Conference on Medical Image Computing and Computer-Assisted Intervention*, volume 1, pages 483–490, 2004.
- [10] C. Fosgate, H. Krim, W. Irving, W. Karl, and A. Willsky. Multiscale segmentation and anomaly enhancement of sar imagery. *IEEE Transactions on Image Process*, 6(1):7–20, 1997.
- [11] Y. Ge, J. Fitzpatrick, B. Dawant, J. Bao, R. Kessler, and R. Margolin. Accurate localization of cortical convolutions in mr brain images. *IEEE Transactions on Medical Imaging*, 15(1):418–428.
- [12] A. Grunerbl, K. Fritscher, M. Blauth, V. Kuhn, and R. Schubert. Shape based 3D level-set segmentation of the proximal femur in ct-data. *available at <http://ftp.informatik.rwth-aachen.de/Publications/CEUR-WS/Vol-264/p091.pdf>*.
- [13] D. Guo and P. Richardson. Automatic vessel extraction from angiogram images. *IEEE Computers in Cardiology*, 25:441–444, 1998.
- [14] R. Jain, R. Kasturi, and B. Schunck. *Machine Vision*. McGraw-Hill Science, 1995.

- [15] M. Kass, A. Witkin, and D. Terzopoulos. Snakes: Active contour models. *International Journal of Computer Vision*, 1:321–331, 1987.
- [16] Y. Kawata, N. Niki, and T. Kumazaki. An approach for detecting blood vessel diseases from cone-beam ct image. In *In Proceedings of the IEEE International Conference on Image Processing*, pages 500–503, 1995.
- [17] Y. Kawata, N. Niki, and T. Kumazaki. Characteristics measurement for blood vessel diseases detection based on cone-beam ct images. In *In Proceedings of the IEEE Conference on Nuclear Science Symposium and Medical Imaging*, volume 3, pages 1660–1664, 1995.
- [18] C. Kirbas and F. Quek. A review of vessel extraction techniques and algorithms. *ACM Computing Surveys*, 36(6):81–121, 2004.
- [19] D. Magee, A. Bulpitt, and E. Berry. Combining 3D deformable models and level set methods for the segmentation of abnormal aortic aneurysms. In *In Proceedings of British Machine Vision Conference*, pages 333–342, September 2001.
- [20] R. Malladi, J. Sethian, and B. Vemuri. Shape modeling with front propagation: A level set approach. *IEEE Transactions on Pattern Analysis and Machine Intelligence*, 17(2):158–175, 1995.
- [21] D. Nain, A. Yezzi, and G. Turk. Vessel segmentation using a shape driven flow. In *In Proceedings of International Conference on Medical Image Computing and Computer-Assisted Intervention*, pages 51–59, 2004.
- [22] N. Niki, Y. Kawata, H. Sato, and T. Kumazaki. 3D imaging of blood vessels using x-ray rotational angiographic system. In *In Proceedings of the IEEE Conference on Medical Imaging*, volume 3, pages 1873–1877, 1993.

- [23] J. O'Brien and N. Ezquerro. Automated segmentation of coronary vessels in angiographic image sequences utilizing temporal, spatial structural constraints. In *In Proceedings of SPIE Conference on Visualization in Biomedical Computing*, 1994.
- [24] T. O'Donnell, T. Boulton, X. Fang, and A. Gupta. The extruded generalized cylinder: A deformable model for object recovery. In *In Proceedings of the IEEE Conference on Computer Vision and Pattern Recognition*, pages 174–181, 1994.
- [25] T. O'Donnell, T. Boulton, and A. Gupta. A new model for the recovery of cylindrical structures from medical image data. In *In Joint Conference on Computer Vision, Virtual Reality and Robotics in Medicine and Robotics and Computer-Assisted Surgery*, pages 223–232, 1997.
- [26] D. Padfield, J. Rittscher, T. Sebastian, N. Thomas, and B. Roysam. Spatio-temporal cell cycle analysis using 3D level set segmentation of unstained nuclei in line scan confocal fluorescence images. In *In Proceedings of the IEEE International Symposium on Biomedical Imaging*, pages 1036–1039, April 2006.
- [27] C. Park, E. Cho, Y. Kwon, M. Park, and J. Park. Automatic separate algorithm of vein and artery for auto-segmentation liver-vessel from abdominal mdct image using morphological filtering. *Lecture Notes in Computer Science*, 3612:1069–1078, 2005.
- [28] C. Pellot, A. Herment, and M. Sigelle. A 3D reconstruction of vascular structures from two x-ray angiograms using an adapted simulated annealing algorithm. *IEEE Transactions on Medical Image*, 13(1):48–60, 1994.

- [29] D. Pham, C. Xu, and J. Price. A survey of current methods in medical image segmentation. *Annual Review of Biomedical Engineering*, 1998.
- [30] Y. Qi. Segmentation and reconstruction of 3D artery models for surgical planning. Master's thesis, National University of Singapore, April 2008.
- [31] H. Schmitt, M. Grass, V. Rasche, O. Schramm, S. Haehnel, and K. Sartor. An x-raybased method for the determination of the contrast agent propagation in 3D vessel structures. *IEEE Transactions on Medical Imaging*, 21(3):251–262, 2002.
- [32] J. Sethian. Examples of the application of level set methods. *available at [math.berkeley.edu/~sethian/Movies/Movieartery.html](http://math.berkeley.edu/~sethian/Movies/Movieartery.html)*.
- [33] J. Sethian. *Level Set Methods*. Cambridge University Press, 1996.
- [34] J. Sethian. *Level Set Methods and Fast Marching Methods*. Cambridge University Press, 1999.
- [35] J. Sethian and S. Osher. Fronts propagating with curvaturedependent speed: Algorithms based on hamilton-jacobi formulations. *Journal of Computational Physics*, 79:12–49, 1988.
- [36] J.A. Sethian. *Level Set Methods and Fast Marching Methods*. Cambridge University Press, 1999.
- [37] E. Sorantin, C. Halmai, B. Erdohelyi, K. Palagyi, L. Nyul, K. Olle, B. Geiger, F. Lindbichler, G. Friedrich, and K. Kiesler. Spiral-ct based assessment of tracheal stenoses using 3D skeletonization. *IEEE Transactions on Medical Imaging*, 21(3):263–273, 2002.

- [38] H. Strunk, G. Stuckmann, J. Textor, and W. Willinek. Limitations and pitfalls of couinaud’s segmentation of the liver in transaxial imaging. *European Radiology*, 13(11):2472–2482, 2003.
- [39] T. Tozaki, Y. Kawata, N. Niki, H. Ohmatsu, and N. Moriyama. 3D visualization of blood vessels and tumor using thin slice ct. In *In Proceedings of the IEEE Conference on Nuclear Science Symposium and Medical Imaging*, volume 3, pages 1470–1474, 1995.
- [40] B. Trackray and A. Andnelson. Semi-automatic segmentation of vascular network images using a rotating structuring element (rose) with mathematical morphology and dual feature thresholding. *IEEE Transactions on Medical Image*, 12:385–392, 1993.
- [41] R. Whitaker. A level-set approach to 3D reconstruction from range data. *Journal of Computer Vision*, 13(3):203–231, 1998.
- [42] C. Xu and J. Prince. Snakes, shapes, and gradient vector flow. *IEEE Transactions on Image Processing*, 7(3):359–369, 1998.
- [43] C. Xu and J. Prince. Gradient vector flow deformable models. *Handbook of Medical Imaging*, 2000.
- [44] C. Xu and J. L. Prince. Gradient vector flow: A new external force for snakes. In *In Proceedings of IEEE Conference on Computer Vision and Pattern Recognition*, 1997.
- [45] P. Yim, P. Choyke, and R. Summers. Grayscale skeletonization of small vessels in magnetic resonance angiography. *IEEE Transactions on Medical Image*, 19(6):568–576, 2000.